Study on the particulate properties and demineralization behavior of bovine bone granules

Wei Tingting

Doctor Program in Advanced Materials Science and Technology

Graduate School of Science and Technology

Niigata University

Contents

General introduction

1.1 Bone regeneration

Bone regeneration is an intrinsic capacity as a part of the healing process in response to injury, as well as the bone development or bone remodeling throughout life [Compston, 2001; Bates, 2007; Kini and Nandeesh, 2013]. Rough composition of bone is organic phase of 20% in weight or 32% in volume, mineral phase of 70% in weight or 43% in volume, and water [Lee, 1981; Novitskaya et al., 2011]. The organic phase consists mainly of more than 90% of collagen and a small amount of non-collagenous proteins. The predominant constituent of the mineral phase is hydroxyapatite (HAp). Bone regeneration occurs through a series of steps of removal of old bone, replacement with an organic phase newly produced, and subsequent mineralization to fill the organic phase as a matrix with a mineral phase. The last step is referred to as osteoinduction. One of the research subjects in regenerative medicine for bone is focused on the promotion of osteoinduction.

Osteoinduction occurs by the action of bone morphogenetic proteins (BMPs). BMPs are non-collagenous proteins, of which the content is less than 0.1% of total proteins. Since 60% and 15% of BMPs are tightly associated with the mineral phase and collagen, respectively [Sampath and Reddi, 1984], they cannot be readily released from bone. It was known that the implantation of a bone chip could induce the bone regeneration [Urist, 1952; Chalmers and Sissons, 1959], but positive results were

obtained at less than 30% [Urist, 1965]. The reason for such a low rate can be thought that BMPs were not used effectively. Although the mineral phase in the surface of the bone chip implanted may be dissolved by osteoclast cells, the dissolution rate is so slow that most of BMPs could be left in the chip. In order to promote the use of BMPs, it is necessary to accelerate the release of BMPs by the dissolution of the mineral phase, i.e. demineralization.

1.2 Demineralized bone matrix (DBM)

1.2.1 Osteoinduction with DBM

Demineralization is carried out by immersing bone in an acid solution. Proteinaceous tissue remained by demineralization is referred to as demineralized bone matrix (DBM). It has been stated that the use of DBM yielded positive results as high as more than 90% [Urist, 1965; Urist, 1968b]. A lot of in vivo studies on the bone regeneration by implanting DBM have been reported [Glowacki et al., 1981a; Sonis et al. 1983; Kaban et al., 1983; Gepstein et al.,1987; Tiedeman et al.,1991].

Removal of the whole mineral phase is referred to as complete demineralization, and that of part of the mineral phase is referred to as partial demineralization. It is known that the results with DBM obtained by partial demineralization are better than one by complete demineralization [Urist, 1968a; Lewandrowski et al., 1997; Han et al., 2003]. Healing of bone fracture needs a couple of months to be achieved. BMPs in DBM through complete demineralization exist in a state that they can be released readily, and therefore they would be lost before contributing to enough bone

formation. It was reported that DBM with less degree of demineralization resulted in more bone formation. The mineral content remained in DBM may facilitate the calcium deposition [Zhang et al., 1997]. Thus, the partial demineralization is preferred to the complete demineralization.

1.2.2 Preparation of DBM

Doctors or dentists pulverize a piece of bone, followed by sieving to classify the granules pulverized, and then demineralized them to obtain DBM. The pulverization has been performed usually by handwork with a hammer or a mortar with a pestle. This work is complicated, and it takes much time such as one day [Murata et al., 2010]. To modify this situation, Murata et al. have developed an automatic high-speed blade mill [Murata et al., 2010]. This electrically-driven mill is easy to operate and makes it possible to produce bone granules only for one minute. It seems convenient for doctors to use, and therefore it is expected that this mill would be increasingly used in future. Whereas this mill has been developed originally for pulverizing teeth, it can be used for bones. The blades made of zirconia and stainless steel are available.

Demineralization is carried out by immersing a bone specimen generally in an acid solution such as nitric acid or hydrochloric acid at a concentration of 0.3–0.6 mol/L for a given time [Urist, 1965; Urist, 1968b; Zhang et al., 1997; Murata et al., 2010]. DBM obtained is washed, dried, frozen and stored. If demineralization is regarded as the dissolution of the mineral phase in bone, it is natural to consider that the demineralization is influenced by the particulate properties such as particle size, size distribution and shape of bone granules used. Therefore, on the preparation of

DBM, the effects of the particulate properties on the demineralization should be known, as well as on the osteoinduction.

1.2.3 Effect of particle size of DBM on osteoinduction

Glowacki et al. [Glowacki et al., 1981b] classified the granules to obtain a series of size ranges of <75 μm, 75–250 μm, 250–450 μm and >450 μm. The particles which were smaller than 75 μm induced the most new bone than the larger particles. Syftestad and Urist [Syftestad and Urist, 1979] sieved the granules to obtain the size ranges of 44–75 μm^3, 125–250 μm^3 and 500–1000 μm^3. (Some studies used the unit of volume. That is regarded as corresponding to the unit of length of micron). They showed that bone granules in the size range of 125–250 μm^3 lead to the most new bone formation. Shapoff et al. [Shapoff et al., 1980] used the DBM granules in the size ranges of 100–300 μm and 1000–2000 μm. The smaller DBM granules in the range of 100–300 μm lead to more formation of new bone.

Zhang et al. [Zhang et al., 1997a] evaluated the osteoinductive potential of DBM by measuring the change in the degree of calcium content by a cell culture-based bioassay. Among the size ranges of <250 μm, 250–350 μm, 350–550 μm, 550–710 μm and 710–850 μm, the DBM in the size range of 550–710 μm provided for the highest level of calcium deposition. Murata et al. [Murata et al., 2010] showed the most effective size range was 500–1000 μm and gave the reason that the DBM granules in this range may decrease the possibility of phagocytosis by the giant cells and digestion by enzymes. Therefore, bone granules in this size range appear to represent the optimal size range for the osteoinduction.

These date represented in the reports demonstrated that bone particle size has a dramatic effect on the osteoinduction process. It should be noticed that the size ranges reported by these studies were based on the mesh size of the sieves used. The actual size of bone granules may be inconsistent with the mesh size. The studies which report precisely the size of bone granules pulverized cannot be found. Therefore, further investigations will be needed to produce DBM granules.

Murata et al. reported in 2010 that the effective particle size range for osteoinduction was 500−1000 μm [Murata et al., 2010]. Recently, Murata's group uses bone and dentin granules with wider size range of 500–2000 μm, and showed that these granules are effective for improving the osteoinduction [Akazawa et al., 2012a; Akazawa et al., 2012b; Kabir et al., 2015]. It is worthy to investigate the particulate properties over wider size range. Thus, I determined to adopt the particle size range of 500–2000 μm for characterization in this study.

1.2.4 Effect of particle size of DBM on demineralization

Demineralization process can be represented by the change of calcium content with time. In the preparation of the partial DBM, the best performed DBM with the desirable calcium content will be needed with considering the effect of particle size. The reports about this study are not so many. Zhang et al. [Zhang et al., 1997] showed DBM with different particle size contained different calcium content. The smaller bone granules are more easily demineralized than larger bone granules, because the smaller granules with larger specific surface area will dissolve more calcium than the larger granules with the same mass or volume per unit time. To get the same calcium

content, demineralizing conditions may be different from the bone granules in different particle size. Thus, it is needed to investigate more about the effect of particle size on demineralization, namely the relationship of the particle size and the calcium content remained in DBM during demineralization.

1.2.5 Kinetics of demineralization

To investigate the relationship between the particle size and the calcium content remained in DBM, it is necessary to know the principle of demineralization. The demineralization process can be described as: movement of acid toward the surface of bone granule from the bulk, movement of acid into the organic matrix toward the minerals, reaction with the minerals at the interaction front, outward movement of reaction product in the organic matrix and movement into the solution.

It is referred that this process can be described as a diffusion and reaction process [Birkedal-Hansen, 1974a] [Lewandrowski et al., 1996]. These studies showed the diffusion of acid in the organic matrix was much slower than the diffusion of acid in the solution, so the diffusion in organic matrix was regarded as the rate controlling step.

(1) Diffusion model

This phenomenon in organic matrix can be expressed by differential equations as:

$$D_{\mathrm{e}} \frac{\mathrm{d}^2 C}{\mathrm{d}\, x_{\mathrm{f}}^{\ 2}} = r(C), \tag{1-1}$$

where on the right-hand side of the equation, $r(C)$ is the demineralization rate and C is

the concentration. On the left-hand side, D_e is the diffusion coefficient and x_f is the penetration distance. This equation describes a simple diffusion process that the diffusion rate of the substance in organic matrix is a function of the penetration distance of acid. This equation can be used when the bone is treated as a sufficiently large flat plate. If a bone block was shaped into a cylinder, the demineralization rate can be fitted to the equation as:

$$D_e \frac{1}{x_c} \frac{d}{d x_c} \left(x_c \frac{d C}{d x_c} \right) = r(C), \tag{1-2}$$

where on the left-hand side of this equation, x_c is the distance from the central axis.

The two equations were applied for the given shapes of bone blocks of a few millimeters in size. Birkedal-Hansen [Birkedal-Hansen, 1974b] showed both of the two specimens reached the complete demineralization. The degree of demineralization can be easily obtained by measuring the penetration distance of one bone block. However, if the irregular bone granules are supposed as the approximate shape of flat plane or cylinder, inconsistencies would occur in the measurement of the penetration distance. The problem is that the penetration distance must be different from granule to granule with variable sizes and shapes, resulting in the difference in the degrees of demineralization of granules. Further, the studies on demineralization behavior need a certain number of bone granules. It is hard to measure the penetration distance for each of the bone granules. Therefore, this model may not fit for all specimens such as bone granules. It is needed to develop another method that can be fitted for the irregular shape granules from different size fractions.

(2) First order equation

As a requirement for calculating the kinetics of any reaction, the reaction order should be known. The rate equation was used to determine the kinetic parameters for demineralization as

$$\text{Rate} = -\frac{\mathrm{d}[\mathrm{Ca}]}{\mathrm{d}\,t} = k[\mathrm{Ca}]^n, \tag{1-3}$$

where k is the rate constant of the reaction and is a function of the acid concentration and temperature, [Ca] is the calcium content in bone, which is defined as the ratio of calcium content remained in DBM per the initial calcium amount in bone [–], and n is the order of the reaction. This equation describes that the rate of decrease in calcium content is proportional to the remaining (unreacted) calcium in bone. Castro-Ceseña et al. [Castro-Ceseña et al., 2011] obtained a linear relationship by plotting the demineralizing rate. Based on this result, Castro-Ceseña et al. indicated that demineralization of bone blocks were fitted for the first order equation.

The first order equation can be applied to find the relationship of the calcium concentration dissolved and the demineralizing time t. If one attempts to find the relationship between the calcium content and the particulate properties, this equation can be easy to be modified with the combination of the specific surface area. This model may be adequate for the expectation that one equation can be fitted for the granules in different particle sizes.

1.3 Subjects to be studied

1.3.1 Characterization of particulate properties of bone granules

Studies on the osteoinduction with DBM should be made by using DBM with the same degree of demineralization to compare the results properly. The degree of demineralization may be varied with the particle size. However, previous studies describe just the size range of sieves used for classifying the bone granules pulverized. Any study which characterizes the particulate properties of individual granules in detail cannot be found.

Now, the most common method for particle sizing is the use of an apparatus based on laser diffraction [Black et al., 1996]. However, such an apparatus is so expensive that it cannot be installed in every clinic. There exists an issue that the refractive index must be input as only one value, although bone is a composite of the mineral phase with proteins, of which refractive indices are quite different from each other. Pulverized granules never have a regular shape like sphere or cube, and the information on the irregularity cannot be output.

Image analysis is an adequate method for characterizing the particulate properties of such irregular-shaped, composite particles. Whereas it used to require using a workstation for image analysis a few decades ago, even free software on a personal computer can run with enough performance at present. Thus, this method is inexpensive and convenient for all clinics and laboratories. Image analysis has been successfully used for characterizing anisotropic specimens in the areas of agriculture

[Cruvinel et al., 1999; Igathinathane et al., 2008; Igathinathane et al., 2009; Mazzoli and Favoni, 2012]. It is expected to be applicable for bone granules.

As described in Section 1.2.3, the particle size range of bone granules adopted in this study was determined to be 500–2000 μm When the granules as-pulverized are dispersed on a flat plate, the height difference between the highest and the lowest granules is more than 1000 μm. Some granules should be out of focus, because an optical microscope system to be used in this study has the depth of focus of about 710 μm at maximum [Private communication from the manufacturer, Shimadzu Rika Corporation]. To observe all granules with their obvious outlines, the bone granules pulverized will be classified into three fractions. The observation in each fraction should make all granules in a field of view be in focus.

The particle size distribution of each fraction can be obtained by this procedure. To obtain a distribution over the whole range as for one specimen, it is needed to plan an approach for integrating the resulting distributions of the three fractions. In this study, it will be proposed that the distributions from image analysis should be integrated by weighting them with the mass fraction from sieving. A report on the characterization by this procedure cannot be found in the literature.

1.3.2 Characterization of demineralization behavior of bone granules

The promotion of osteoinduction with DBM is dependent on the calcium content, i.e. the degree of demineralization. However, it has not been known yet how much degree of demineralization is the most effective on osteoinduction. To fix it, still more animal experiments have to be done by researchers in the area of regenerative

medicine. Studies in materials engineering may contribute to the establishment of the formulation for preparing DBM with desirable properties.

It has been reported that the particulate properties of bone granules affect the demineralization behavior as described above. However, they have to be reevaluated, because the characterization of the particulate properties in their studies was not reliable enough. The characterization procedure will be established in the first part of this study. Based on this result, the relation of the demineralization behavior with the particulate properties should be discussed.

1.4 Objectives

As described above, the characterization of demineralization behavior of bone granules has been reported. However the report on the relationship between calcium content remained in DBM and particulate properties is rarely seen. One objective of this study is to characterize the particle size of the individual bone granule obtained by pulverization and to evaluate particle size distribution. An approach to express the particulate properties such as particle size, particle size distribution will be proposed, and the relationship between the particle size or size distributions and the pulverization conditions will be discussed. In addition, the particle shape of bone granules will be evaluated to find the relationship between the particle shape of pulverized bone granules and the pulverizing conditions.

When doctors and dentists carry out the animal experimentations to investigate the effectiveness of partial demineralization, DBM with the same degree of

demineralization should be used. The other objective of this study is to propose how to determine the demineralization condition to obtain the same degree of demineralization. The demineralization behavior of the bone granules will be examined and the change in the degree of demineralization with time will be tried to fit a demineralization rate equation with consideration of the particulate properties.

1.5 Outline of this thesis

Chapter 1 is this chapter, in which the background of bone regeneration with DBM was introduced. The objectives of this thesis were set as to characterize the particulate properties of bone granules and to characterize their demineralization behavior.

In Chapter 2, bovine bone will be pulverized with a high-speed blade mill, and the particulate properties of each granule will be characterized by combining the results from both sieving and image analysis.

In Chapter 3, the pulverized bovine bone granules will be demineralized in an acid solution. The demineralization behavior will be discussed by fitting a kinetics model with consideration of the particulate properties characterized in Chapter 2.

In Chapter 4, the general conclusions of these studies will be summarized.

Nomenclature

C	concentration [mol/L]
D	diffusion coefficient
k	rate constant
n	order of the reaction
r	demineralizing rate
t	demineralizing time [h]
x	penetration distance [μm]
[Ca]	calcium content [–]

Subscripts:

c	cylinder
e	diffusion
f	flat plate

Particulate properties of bovine bone granules

2.1 Introduction

In this chapter, bovine bone granules are prepared by pulverizing a bone block with an automatic mill and classified by sieving into three fractions. The size and shape of individual granules are analyzed by image analysis. A new approach is proposed, by which the particle size distribution is expressed by combining the results from sieving and image analysis. The relationship between the average particle size and aspect ratio is discussed.

2.2 Experimental procedure

2.2.1 Pulverization

Bone from bovine femur was frozen and cut into blocks of 20 mm x 20 mm x 10 mm in size. The pulverizer used was a high-speed blade mill (Hayasaka Rikoh Co., Ltd., Sapporo, Japan). As shown in Fig. 2-1, it was constructed of a crushing blade of 73 mm long, 8 mm wide, and 7.5 mm high and a vessel, both of which were made of stainless steel.

A bone block was put into the vessel and then buried with ice blocks of 10 mm cube made of normal saline. The mill was driven for a pulverizing time of 60 or 120 s at a revolution speed of 6000, 8000, or 10000 rpm. The ice blocks were melted

completely during 60 s, so that the specimen pulverized was obtained as slurry. This slurry was filtrated with a filter paper of No. 5A and washed with pure water five times. The bone granules obtained were dried in a desiccator. The pulverization was performed four times under each condition.

2.2.2 Sieving

The granules dried were sieved on a vibratory sieve shaker (Model AS 200 digit, Retsch GmbH, Haan, Germany) under the following conditions: time for 15 min, amplitude of 40, and interval for 10 s. Each fraction classified was weighed and then stored in a freezer.

Standard sieves of 500, 710, 1000, and 2000 μm in mesh size were used, which are referred to as Sieves 1–4 hereafter. Specimens remained on them are referred to as Fractions I–IV, respectively. The effective mass was defined as the total mass of Fractions I–III. The yield was defined as the ratio of the effective mass to the total mass of all fractions:

$$Y = \frac{\sum_{i=1}^{3} m_i}{\sum_{i=0}^{4} m_i}, \tag{2-1}$$

where i is the index of the fraction. The initial index $i = 0$ designates the specimen remained in the receiver. The mass percentage of the ith fraction was defined as

$$M_i = \frac{m_i}{\sum_{i=1}^{3} m_i}, \tag{2-2}$$

where m_i is the mass of granules in the ith fraction. In general, the frequency f_i of the histogram can be calculated by

$$f_i = \frac{1}{x_{i+1} - x_i} \times M_i \,, \tag{2-3}$$

where x_i is the mesh size of Sieve i and the term $(x_{i+1} - x_i)$ shows the width of the ith fraction. In order to fix the height of the highest rectangle of the histogram to be unity, the frequency was normalized as follows:

$$F_i = \frac{f_i}{f_{\max}} \,, \tag{2-4}$$

where $f_{\max}$ is chosen as the largest value of f_i. The histogram of the specimens from sieving was drawn by using F_i, corresponding to volume-mean distribution. In this histogram, the area of the rectangle of each fraction can be calculated by

$$A_i = F_i \times (x_{i+1} - x_i) \,. \tag{2-5}$$

2.2.3 Image analysis

The granules were scattered on a glass plate and examined with an optical microscope. They show the pulverized granules are anisotropic in the particle shape. A typical micrograph is shown in Fig. 2-2(A), the binarized image is shown in Fig. 2-2(B). The projection of each granule was identified, and each area was calculated. Characteristic lengths a and b are the major and minor axes of the fitted ellipse to the projection. The equivalent circle of which the area is the same as the projection was found to determine the particle size d, or Heywood diameter. The average particle size D was determined to be the area mean size defined as

$$D = \frac{\sum d^2}{\sum d}, \tag{2-6}$$

where $\sum$ means the summation for all granules. On the other hand, the smallest circumscribed ellipse for each granule was found, and the major and minor axes were defined as the characteristic lengths *a* and *b*, respectively. The aspect ratio *r* was defined as

$$r = a / b. \tag{2-7}$$

The average aspect ratio *R* was obtained by weighting with each area:

$$R = \frac{\sum rd^2}{\sum d^2}. \tag{2-8}$$

By hypothesizing, a plane was normal to the direction of the axis *a*, the projection was obtained. The maximum length viewed under the microscope can be identical to the length *b*, or Feret diameter, as shown in Fig. 2-2(C). The maximum length normal to the axis *b* is defined as another characteristic length *c*, although its value cannot be measured by the direct observation under a microscope.

Each fraction was divided into some subfractions of which the width was 100 μm. The characteristic diameter of the granule in a subfraction was defined as the median diameter D_{cj}:

$$D_{cj} = \frac{x_j + x_{j+1}}{2}, \tag{2-9}$$

where *j* is the index of the subfraction. The total area s_j of the granules in the *j*th subfraction was calculated by

$$s_j = \frac{\pi D_{cj}^{\ 2}}{4} \times n_j, \tag{2-10}$$

where n_j is the number of the granules.

An original histogram can be drawn from the frequency f_j:

$$f_j = \frac{s_j}{\sum s_j}, \tag{2-11}$$

where $\sum$ means the summation in all subfractions. The area of the rectangle of each subfraction in this histogram is $f_j(x_{j+1} - x_j)$. In order to compare the histograms from sieving and image analysis, the total area of the rectangles of subfractions in the *i*th fraction should be made equal to the area A_i of the rectangle of the *i*th fraction. Therefore, f_j was reduced to obtain

$$F'_j = f_j \times \frac{A_i}{\sum\{f_j(x_{j+1} - x_j)\}}. \tag{2-12}$$

Three normalized histograms for Fractions I–III can be drawn by using F'_j for the ordinate. The overall frequency of each subfraction can be obtained by weighting with the mass percentage of the corresponding fraction:

$$F''_j = \sum_{i=1}^{3}(F'_j \times M_i). \tag{2-13}$$

An integrated histogram regarding all subfractions can be drawn by using F''_j. Finally, in order to make the total area of the two histograms equal, the frequency was normalized as

$$F_j = F''_j \times \frac{\sum_{i=1}^{3} A_i}{\sum\{F''_j(x_{j+1} - x_j)\}}. \tag{2-14}$$

These procedures of characterization were performed for more than 200 granules. The significant difference was examined by *t*-test.

2.3 Results and discussion

2.3.1 Conventional evaluation of particle size

The optical micrographs of the specimens from Fraction I to III pulverized at 10000 rpm for 60 s are shown in Fig.2-3. They show the pulverized granules are anisotropic in the particle shape. Table 2-1 lists the results of the specimens of the three fractions pulverized at 10000 rpm for 60 s and 120 s. Fig. 2-4(A) shows a histogram made from the results of the specimen (A) in Table 2-1. The frequency was reduced nearly by 0.88 from Fraction I to Fraction III. Compared Fig. 2-4(B) with Fig. 2-4(A), it is seen that the extension of the pulverizing time from 60 s to 120 s resulted in the increase in the frequency of Fraction II and the decrease in that of Fraction III. Compared Fig. 2-4(C) with Fig. 2-4(A), it is found that the decrease in the revolution speed from 10000 rpm to 6000 rpm caused the increase in the frequency of Fractions II and III.

Fig. 2-5 shows the changes in the average particle size calculated by Eq. (2-6) with pulverizing time. The average particle size of the specimen pulverized at 10000 rpm for 60 s was 1275 μm, and it was decreased to 1148 μm for 120 s. A significant difference ($p<0.05$) was recognized between these values. With decreasing revolution speed, the average particle size was increased to 1552 μm at 6000 rpm for 60 s. Fig. 2-6 shows the change in the yield with pulverizing time. This figure also illustrates the decreasing tendency as shown in Fig. 2-5. It is found that the pulverization for a longer time at a higher speed has increased the production of granules collected in the receiver to be discarded.

Fig. 2-7 shows the change in the average aspect ratio with pulverizing time. At a pulverizing time of 60 s, the average aspect ratio was 1.57, 1.53 and 1.49 at a revolution speed of 6000, 8000 and 10000 rpm, and it was decreased to 1.53, 1.47 and 1.42, respectively, with extending the pulverizing time to 120 s. For the same pulverizing time, the aspect ratio was decreased with increasing the revolution speed. It shows that pulverizing at a slower revolution speed leads elongated granules.

It is easy to understand that these are common-sense results, but it is hard to get more information. In order to know the pulverization behavior of bovine bone in detail, it is necessary to develop an alternative procedure for evaluating the characteristics.

2.3.2 Evaluation of particle size by image analysis

Fig. 2-8 shows histograms of the specimen pulverized at 10000 rpm for 60 s. The black rectangles are individual results of Fractions I–III from sieving as illustrated in Fig. 2-4, whereas the heights of them were fixed to be unity. The grey rectangles are the results from image analysis, of which the abscissa is the Heywood diameter *d*. The frequency of them was obtained by using Eq. (2-12). These two distributions appear quite different from each other. In Fig. 2-8(A) for Fraction I, it is found that most of the granules are larger than the mesh size of the immediately upper sieve. Hereafter, granules larger than the upper limit of the belonging fraction are referred to as L particles. The amount of granules within the objective particle size range is very small. Granules from the lower limit to the upper limit of the fraction are hereafter referred to as M particles. A little amount of granules less than the lower limit was also

observed, which are referred to as S particles. The same tendency was recognized for Fraction II as shown in Fig. 2-8(B). Although the distribution by grey rectangles in Fig. 2-8(C) resembles that by the black rectangle, S and L particles still exist. It can be easily understood that the S particles are remained by adhering on some of M particles. To understand the existence of L particles, it is necessary to take into account the non-equiaxed shape of bone granules as described below.

In this study, each granule is specified by three lengths *a*, *b*, and *c*, defined in Fig. 2-2. The lengths *a* and *b* are measured with a microscope, whereas *c* cannot be measured. However, it can be known that *c* is the shortest because the granules placed on the stage of the microscope should be the most stable state by directing the shortest axis normal to the microscope. Therefore, the order of them is recognized to be $a > b > c$. If these were recognized to be of an equiaxed shape, e.g. cubic or spherical, their volume would be estimated much larger than the actual volume. Thus, it is found that the expression of the particle size distribution in terms of volume is not proper for such non-equiaxed granules, even if this is the most popular manner.

Fig. 2-9(A) illustrates a situation in which a granule passes through the upper sieve of x_{i+1} in mesh size and remains on the lower sieve of x_i in mesh size. This granule will be accompanied in a fraction with the size range between x_i and x_{i+1}, which is named as the *i*th fraction. The longest length *a* is not concerned with the result of sieving, when the granule makes the *a* axis direct to the sieve. Since a granule with the length *a* larger than x_{i+1} can pass through the sieve, the characteristic diameter *d* may become larger than the mesh size. This is the reason for

the existence of L particles.

A granule with the length *b* smaller than x_{i+1} can pass through Sieve *i*+1. It will remain on Sieve *i* when *b* is larger than x_i, as shown in Fig. 2-9(B). Thus, the second long length *b* is the determining length, as reported in theoretical and empirical studies [Allen, 2003]. Based on this consideration, the validity of the results of sieving must be proved with the particle size distribution expressed by *b* as the abscissa.

Fig. 2-10 illustrates the same results as Fig. 2-8, but the Feret diameter *b* is used for the abscissa instead of the Heywood diameter *d*. The distribution ranges became similar to the ranges between x_{i+1} and x_i for all fractions, although a portion over x_{i+1} still exists. The size of the diagonal of the sieve is the square root of two times as long as the mesh size. A granule with *b* less than the diagonal of Sieve *i*, i.e. $b < \sqrt{2}x_i$, may pass through it, as shown in Fig. 2-9(C).

The broken lines in Fig. 2-10 designate the square root of the upper limits: 1004, 1414, and 2828 μm for Fractions I, II, and III, respectively. It is found that the largest size is confined to $\sqrt{2}x_{i+1}$ in all fractions. From this treatment, the results of this study are confirmed to be proper.

Granules with $b \approx \sqrt{2}x_{i+1}$ should have an acute angle at the edge of the *b* direction. Such a sharp edge is one of the characteristics of pulverized granules of hard, brittle materials. Furthermore, since bone originally has a laminar structure of the inorganic ingredients and collagen stacking, the edges are prone to be sharpened. The existence of a lot of granules in the range from x_{i+1} to $\sqrt{2}x_{i+1}$ reflects the characteristics of bone. It can be concluded that the combining sieving and image

analysis is practical to evaluate anisotropic granules like bone. Thus, it was shown that the Feret diameter *b* is useful to understand the result. However, *b* is not adequate to be used as a characteristic diameter for expressing the particle properties because it does not include information on *a*. The Heywood diameter *d* will be used in the following description.

Fig. 2-11(A) shows the particle size distribution obtained according to Eq. (2-14). Granules larger than 2000 μm had to be excluded as Fraction IV, but such large granules are confirmed again to be included. The distribution of the grey rectangles is broader than that of the black rectangle. Figs. 2-11(A) and (B) are the results at a larger revolution speed, 10000 rpm. The sieving indicates that the largest fraction is Fraction I, and the frequency of Fraction III is very small. The image analysis provides Fig. 2-11(B), which is nearly the same distribution around the normal distribution. There are few L particles in Fig. 2-11(B). Fig. 2-11(C) is the result at a slower revolution speed, 6000 rpm. The distribution became much broader. A portion of L particles were increased, so that granules more than 0.80 in frequency at the maximum were observed. As stated so far, it was confirmed that the detailed particle size distribution diagram can be obtained by using the image analysis.

2.3.3 Evaluation of aspect ratio

The bone granules pulverized have an elongated shape as shown in Fig. 2-3. Therefore, an aspect ratio of *a* to *b* was adopted as a scale for expressing the particle shape. Fig. 2-12 shows the relationship between the average particle size *D* from Eq. (2-6) and the average aspect ratio *R* from Eq. (2-8) for Fractions I–III of four

specimens pulverized at 10000 rpm for 60 s. The close and shaded symbols are of M particles and L particles, respectively. The open symbol designates the average of the entire specimen. The data of S particles was omitted, because its existing proportion was too low to consider their contribution. In Fraction I, the aspect ratio was 1.43 for M particles and 1.62 for L particles. Also in Fractions II and III, the aspect ratio of L particles was larger than that of M particles. This result reflects that the L particles are essentially anisotropic in size. The aspect ratio of M particles was not changed for all fractions, whereas that of L particles was the largest for Fraction I. Consequently, a negative correlation between average aspect ratio and average particle size can be recognized. This is dependent on the proportion of L particles having a larger aspect ratio. Although the L particles of Fraction I have almost the same average particle size as the M particles of Fraction II, the average aspect ratio is larger by more than 10%. This result suggests that bone granules would be different in shape even if their size is the same.

Fig. 2-13 shows the relationship between the average particle size and the average aspect ratio of specimens pulverized under different conditions. The average aspect ratio was decreased from 1.44−1.73 to 1.32−1.63 with the increase in particle size from Fractions I to III. Thus, the particle shape can be changed by changing pulverizing conditions. It is suggested that the pulverizing conditions should be chosen according to what use the bone granules would be applied to and what property of them would be desirable for that use.

2.4 Conclusions

Bovine bone was pulverized with a high-speed blade mill, and the size of each granule after sieving was measured by image analysis. Expressing the characteristic diameter by Heywood diameter, the result that granules larger than the mesh size had passed through the sieve was obtained. This result can be explained without any inconsistency by the fact that the Feret diameter was less than the diagonal of the sieve mesh size. It was found that the aspect ratio of the bone granules was changed by the pulverizing conditions. Since sieving is a convenient method, it should have also been used in the future. However, it is insufficient to characterize the diameter by sieving because powders having the same average particle size probably reveal different particulate characteristics. The image analysis was confirmed to be useful as an auxiliary method for investigating the characteristics in detail of granules sieved.

Figures and table:

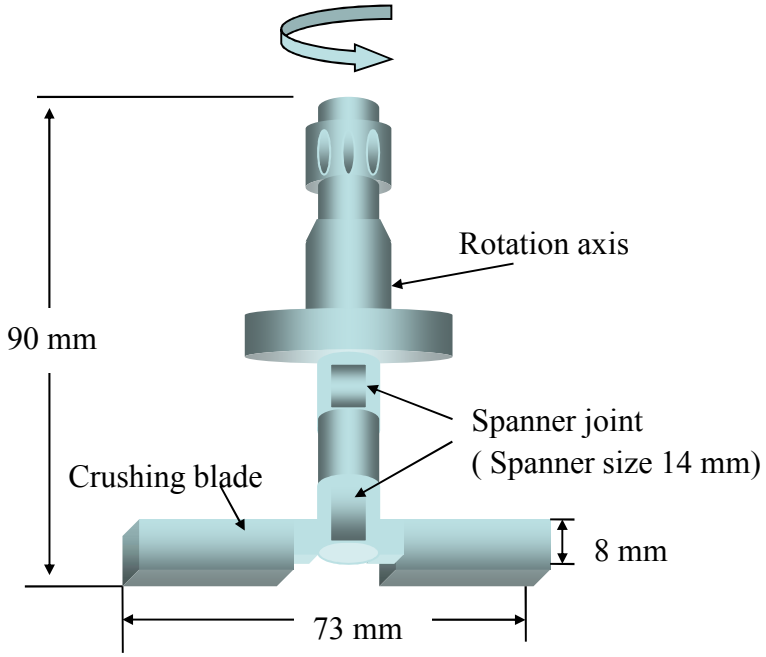

Fig. 2-1 Spiale and blade of the automatic mill.

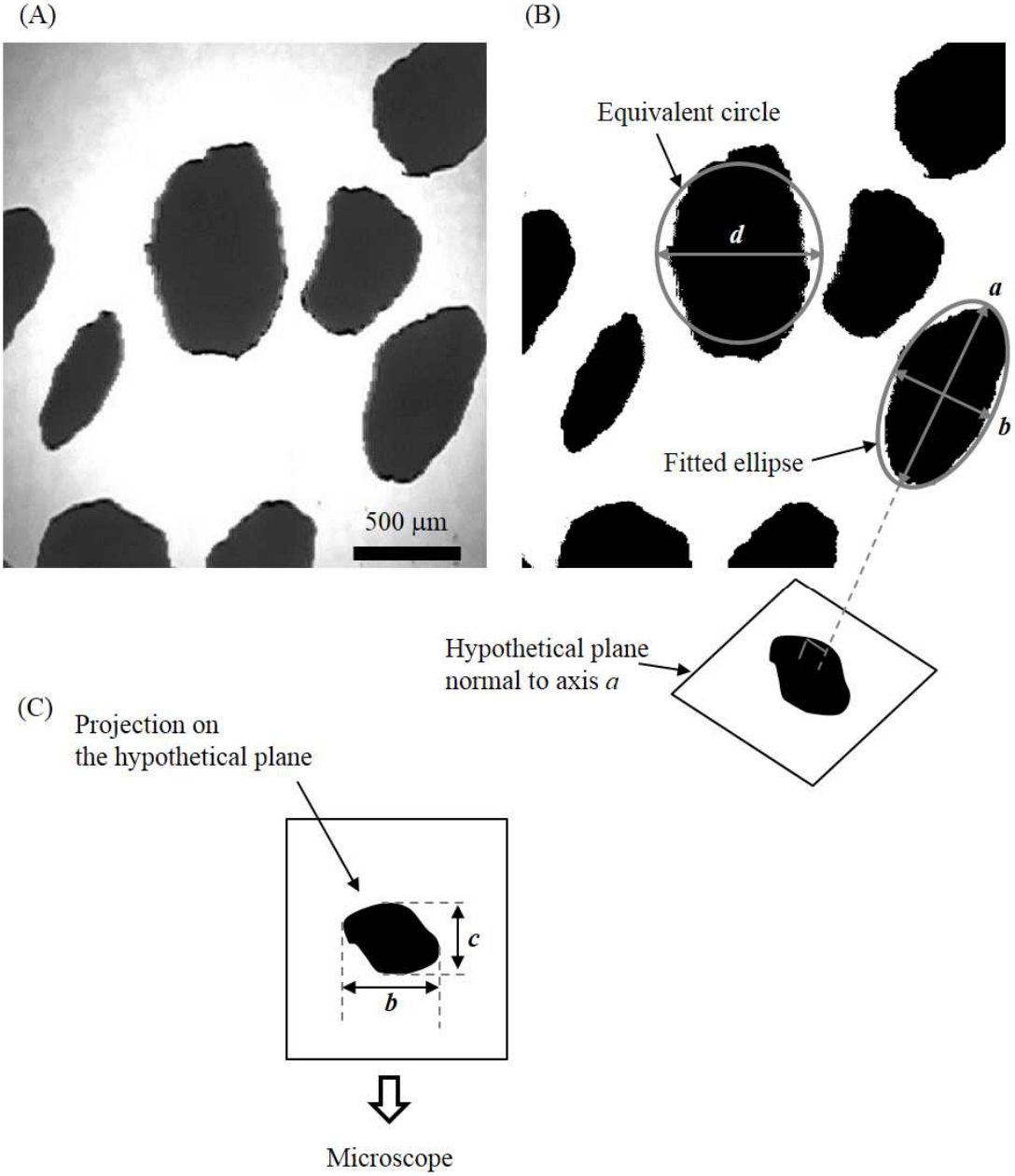

Fig. 2-2. Definition of characteristic lengths. (A) Optical micrograph of bone granules. (B) Binarized image of (A). *d* is the equivalent circle diameter of a projected area, or Heywood diameter. Characteristic lengths *a* and *b* are the major and minor axes of the fitted ellipse to the projection. (C) Characteristic length *c* is defined as the minor axis of the fitted ellipse to a projection on a hypothetical plane normal to the major axis *a*.

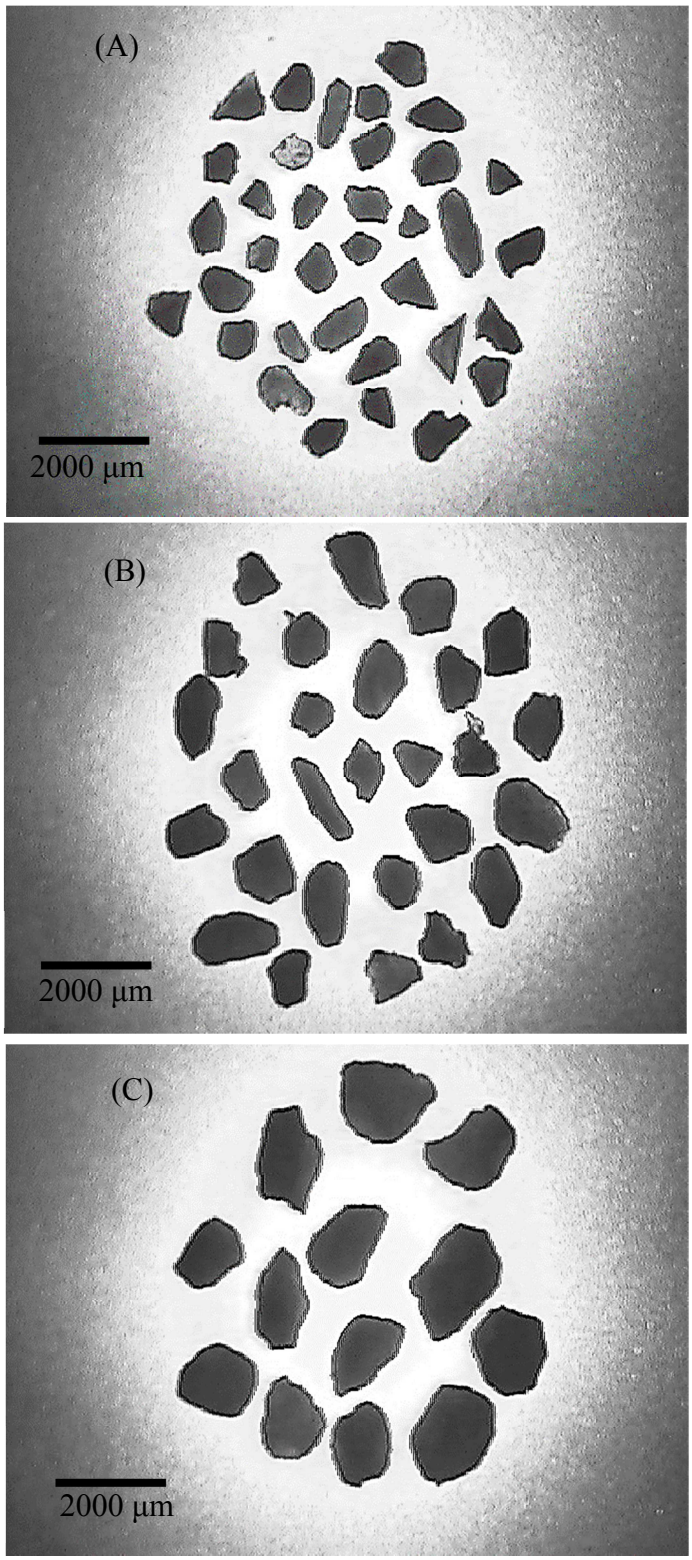

Fig. 2-3 Optical micrographs of the specimens pulverized at 10000 rpm for 60 s. (A): Fraction I, (B): Fraction II, (C): Fraction III.

Table. 2-1 Results from sieving the specimens pulverized at 10000 rpm for (A) 60 s and (B) 120 s.

Fraction	Sieve No.	Mesh size [μm]	Mass [g]	
			(A)	(B)
IV	4	2000	0.75	0
III	3	1000	3.23	0.75
II	2	710	1.15	1.43
I	1	500	0.79	1.75
R	Receiver	–	3.16	5.08
Total mass [g]			9.08	9.01
Effective mass [g]			5.17	3.93
Yield [%]			56.9	43.6

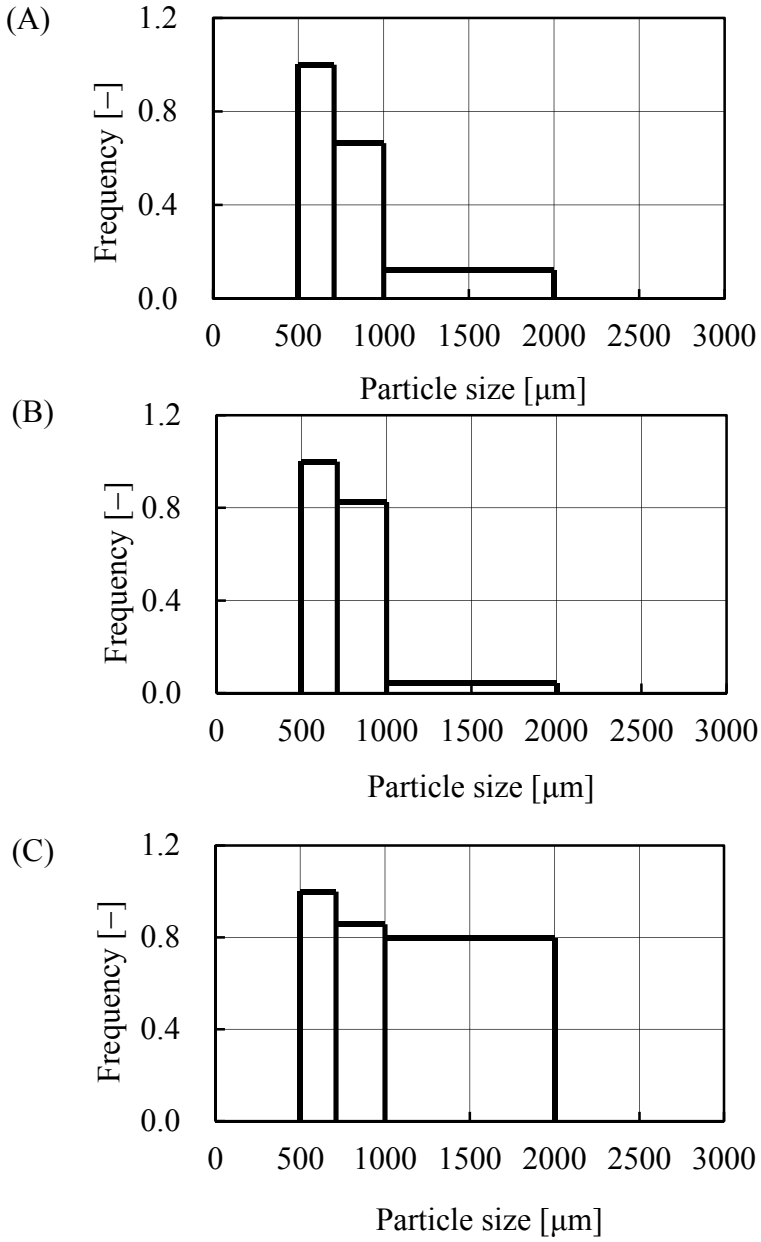

Fig. 2-4. Particle size distribution of the specimens after sieving. Pulverized (A) at 10000 rpm for 60 s, (B) at 10000 rpm for 120 s, and (C) at 6000 rpm for 60 s. Fraction I: 500–710 μm. Fraction II: 710–1000 μm. Fraction III: 1000–2000 μm.

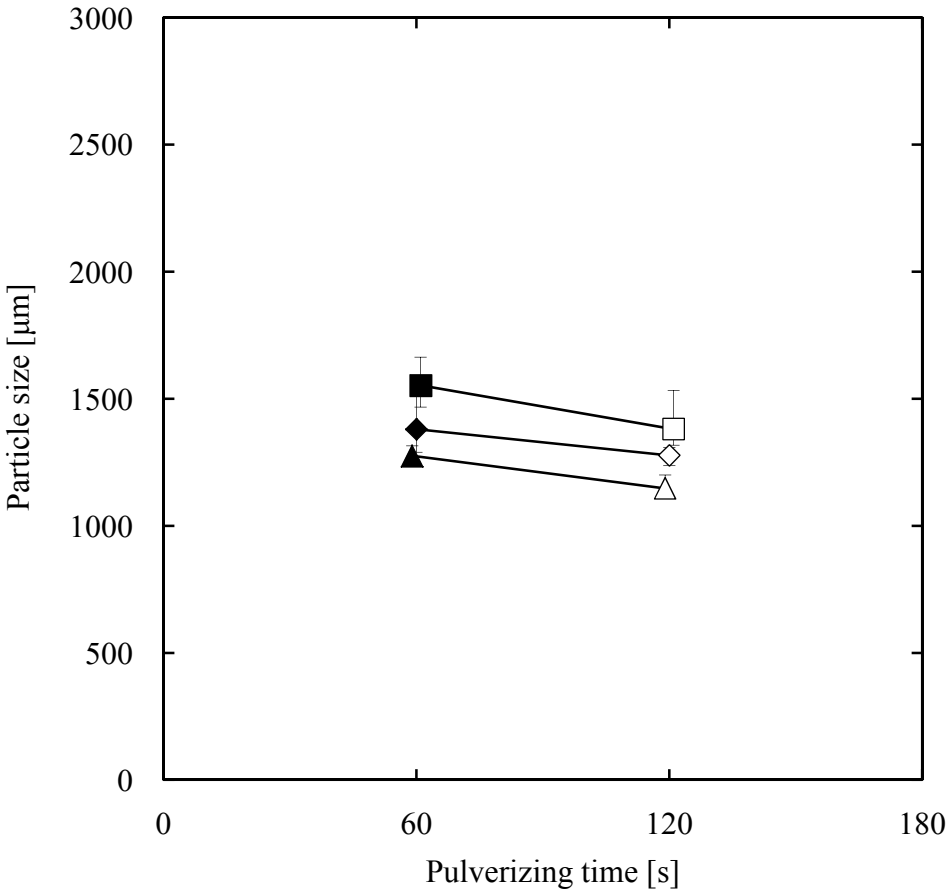

Fig. 2-5. Change in the average particle size with pulverizing time for 60 s (■) or 120 s (□) at revolution speeds of 6000 rpm (■), 8000 rpm (♦), and 10000 rpm (▲).

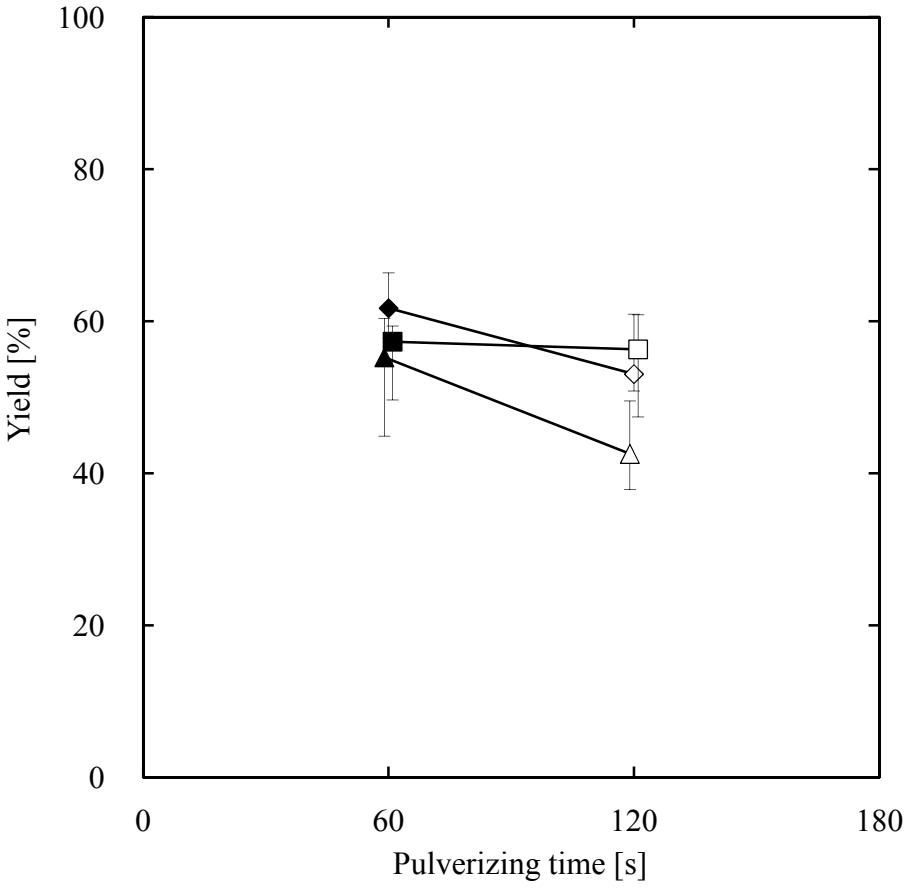

Fig. 2-6. Change in the yield with pulverizing time for 60 s (■) or 120 s (□) at revolution speeds of 6000 rpm (■), 8000 rpm (♦), and 10000 rpm (▲).

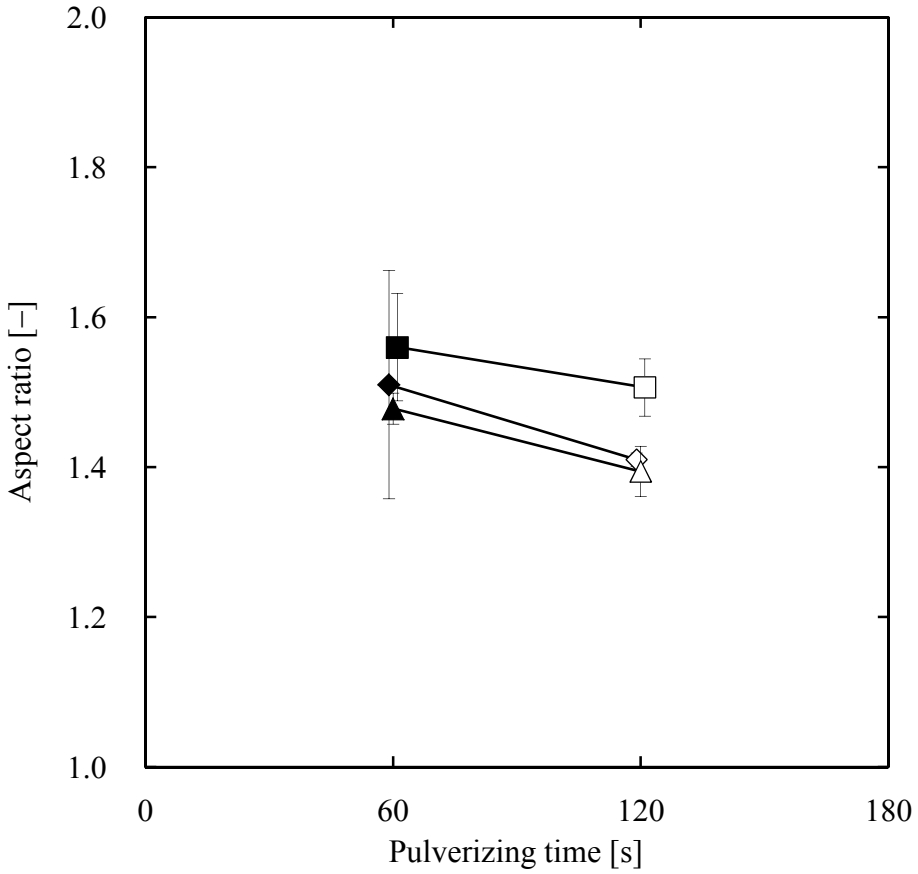

Fig. 2-7. Change in the average aspect ratio with pulverizing time 60 s (■) or 120 s (□) at revolution speeds of 6000 rpm (■), 8000 rpm (♦), and 10000 rpm (▲).

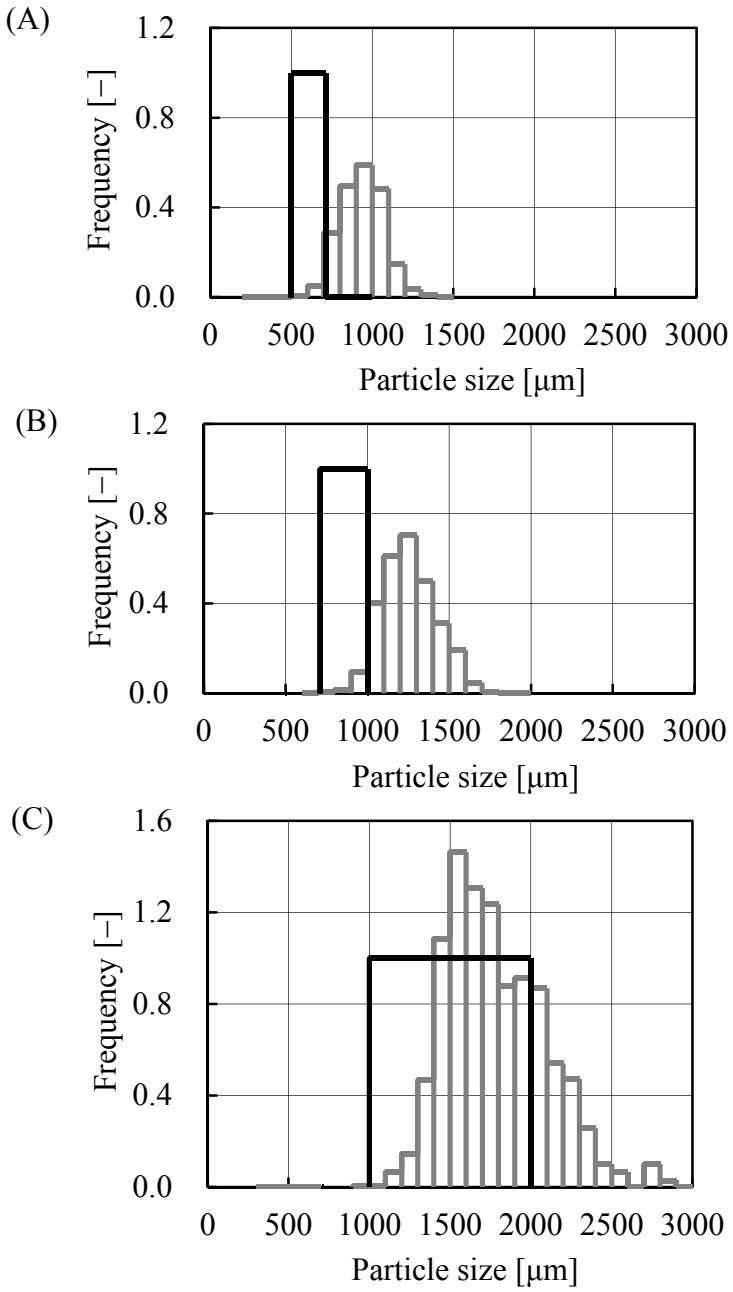

Fig. 2-8. Particle size distribution of the specimen pulverized at 10000 rpm for 60 s.
Black histogram: Particle size distribution from sieving.
Grey histogram: Particle size distribution from image analysis.
(A): Fraction I. (B): Fraction II. (C): Fraction III.

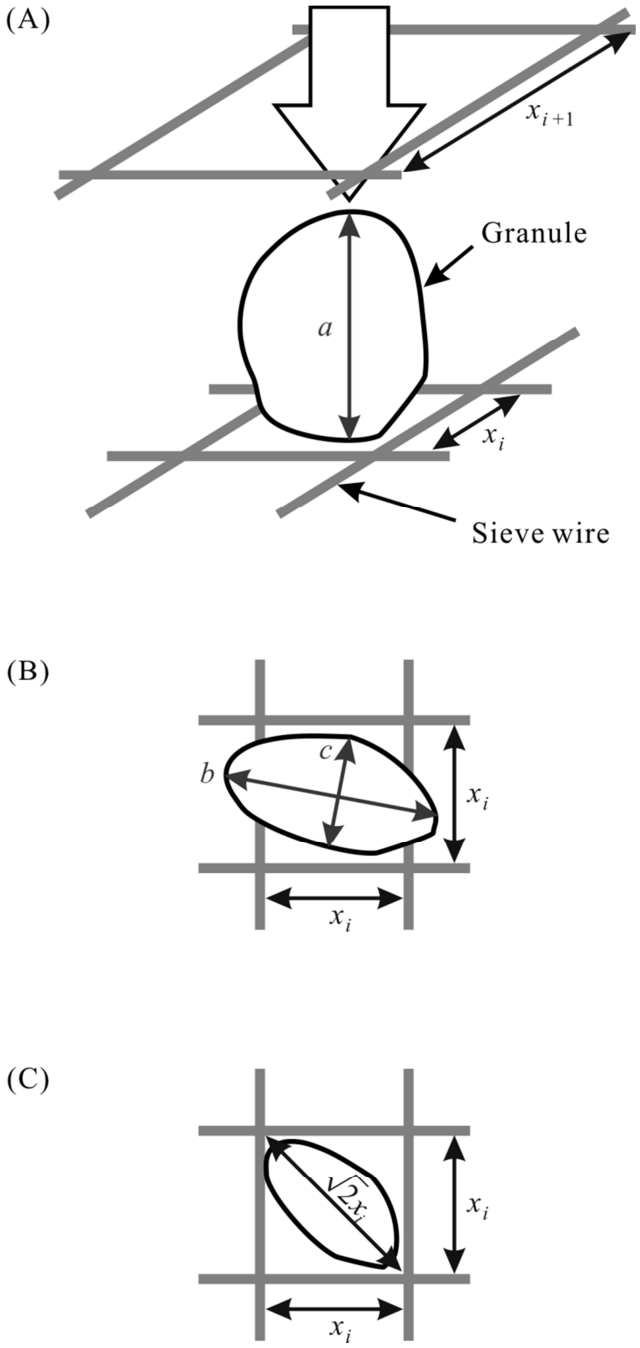

Fig. 2-9. Schematic illustration of a particle passing through a sieve. (A) Concept of passing. The upper limit of sieve is x_{i+1}, and the lower limit is x_i. The longest axis a is directed toward the sieve. (B) When the medium axis b is larger than the mesh opening size and directed along the sieve wire, the particle cannot pass through. (C) If b is less than the diagonal length and the shortest axis c is short enough, the particle may pass through.

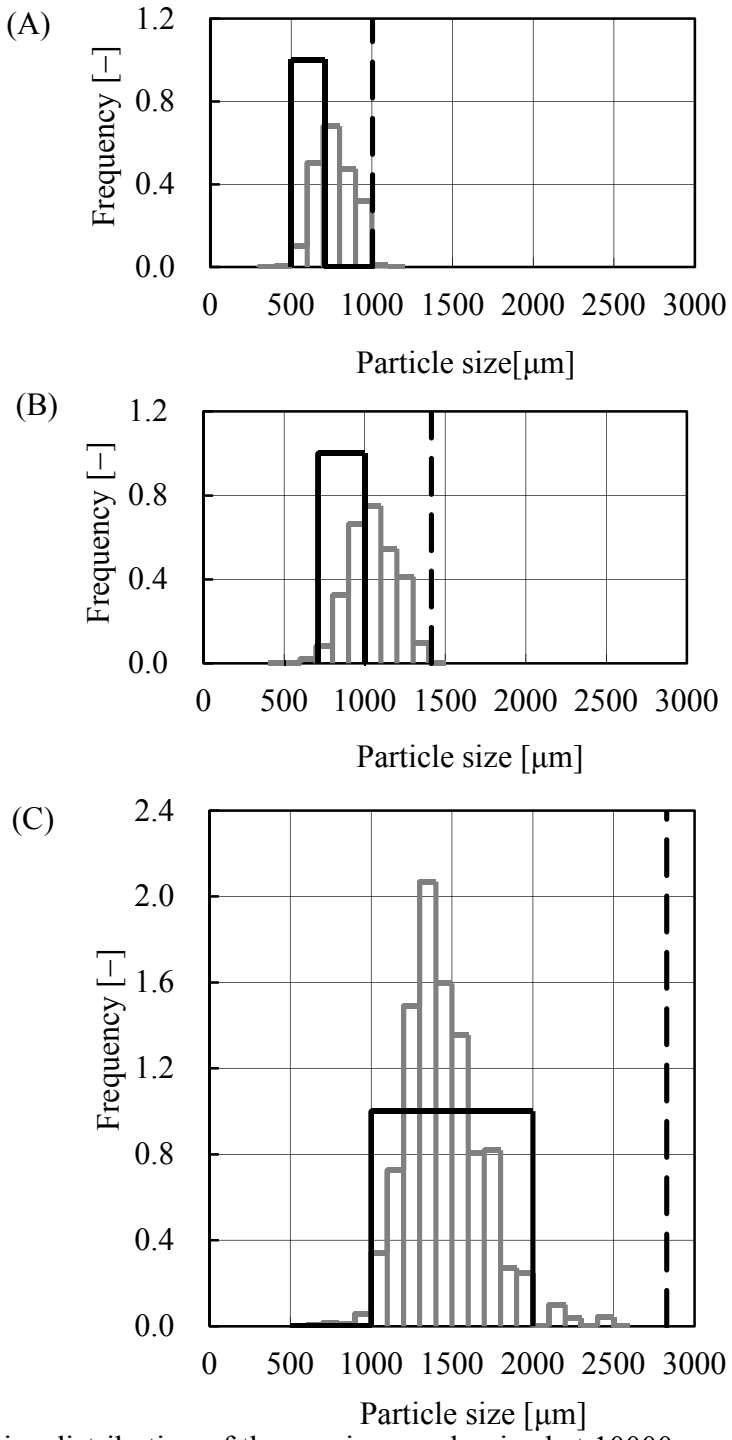

Fig. 2-10. Particle size distribution of the specimen pulverized at 10000 rpm for 60 s. The Feret diameter *b* is used for the abscissa.
Black histogram: Particle size distribution from sieving.
Grey histogram: Particle size distribution from image analysis.
Black broken line: The square root of the upper limits.
(A): Fraction I. (B): Fraction II. (C): Fraction III.

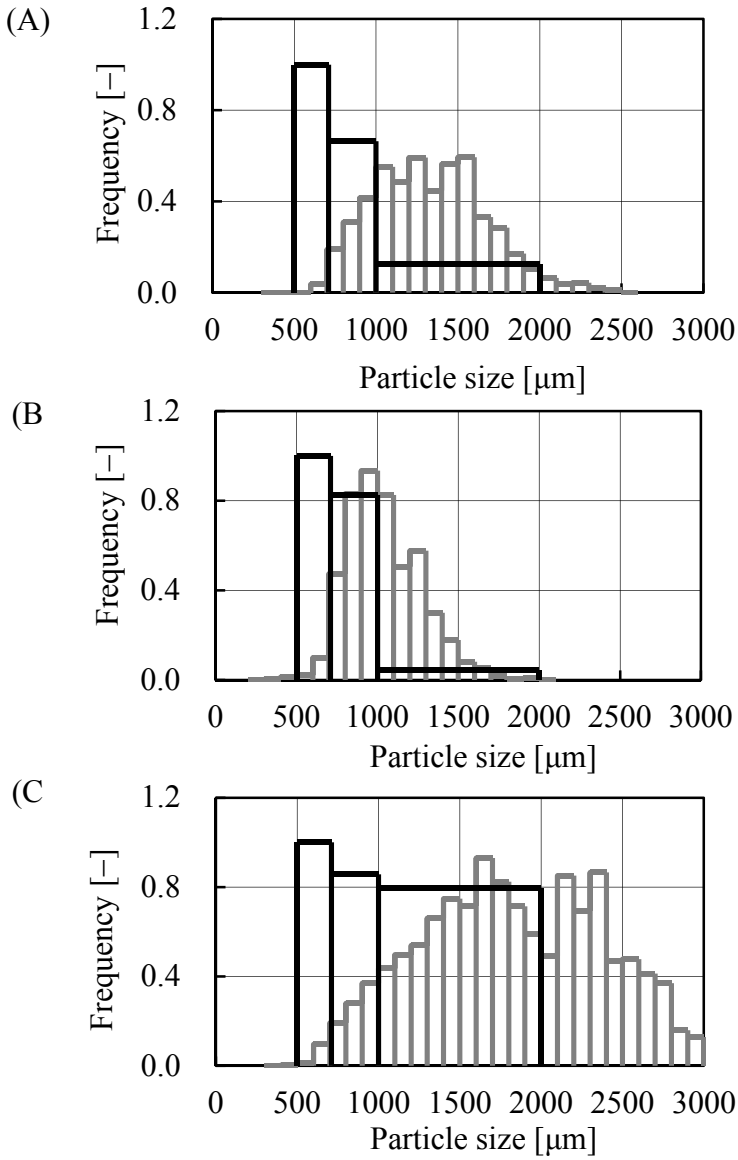

Fig. 2-11. Particle size distribution of the specimens pulverized (A) at 10000 rpm for 60 s, (B) at 10000 rpm for 120 s, and (C) at 6000 rpm for 60 s.
Black histogram: Particle size distribution from sieving.
Grey histogram: Particle size distribution from image analysis.

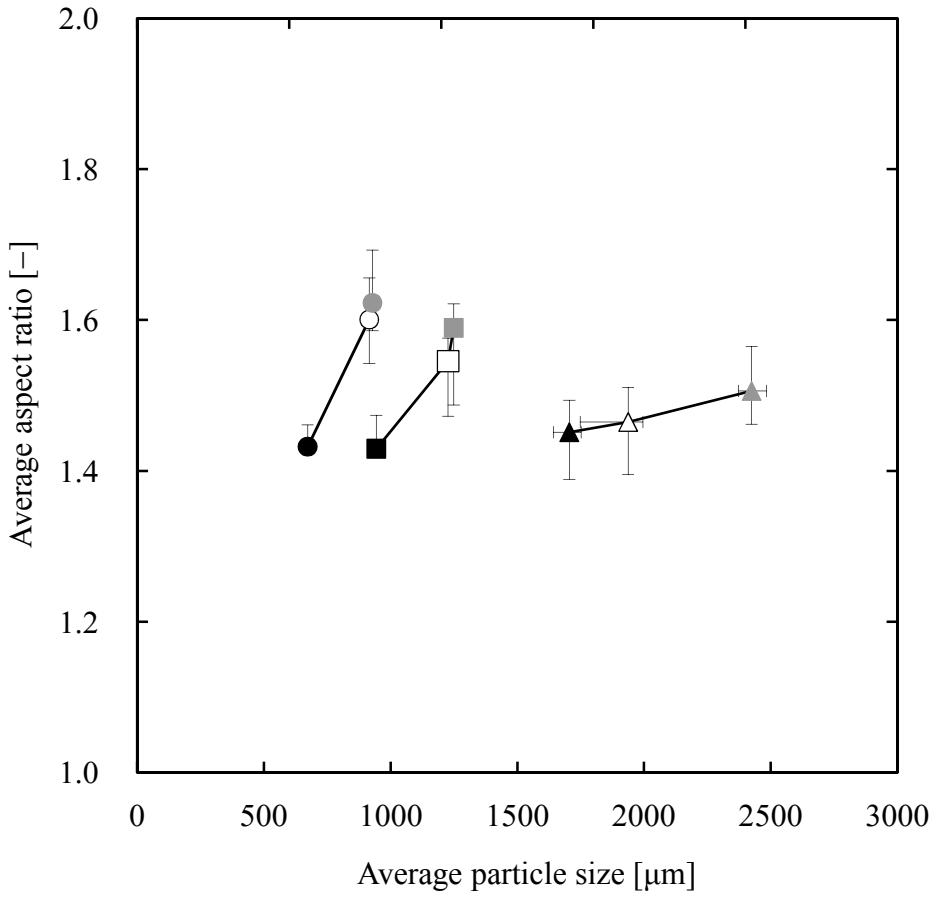

Fig. 2-12. Relationship between the average particle size and the average aspect ratio of Fractions I–III of specimens pulverized at 10000 rpm for 60 s.
●: Fraction I, ■: Fraction II, ▲: Fraction III.
Grey symbol: L particles, open symbol: the average of entire specimens, black symbol: M particles.

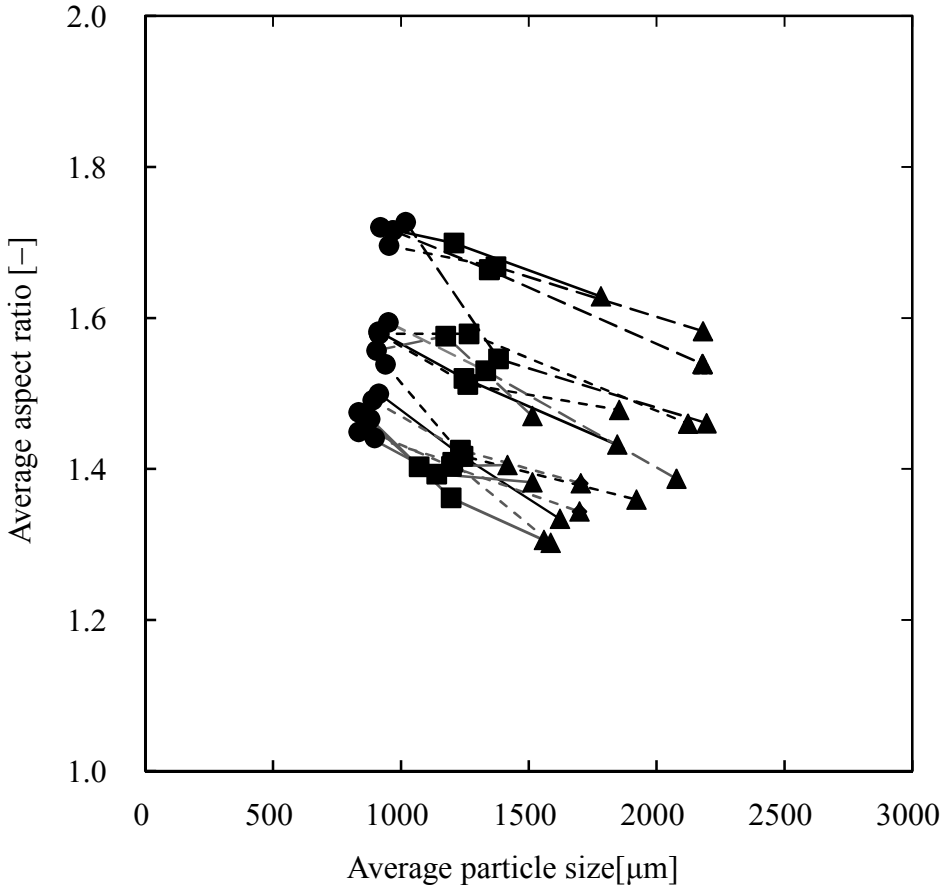

Fig. 2-13. Relationship between the average particle size and the average aspect ratio of Fractions I–III of specimens pulverized at 6000 (broken line), 8000(dotted line) and 10000 rpm for 60 (black line) and 120 s (grey line). ●: Fraction I, ■: Fraction II, ▲: Fraction III.

Nomenclature

a	major axes [μm]
b	minor axes [μm]
c	minor axes normal to a [μm]
d	Heywood diameter [μm]
Dc	average particle size [μm]
f	frequency corresponding to mass [–]
F	frequency corresponding to volume mean [–]
m	mass [g]
M	mass percentage [–]
n	number
r	aspect ratio [–]
R	average aspect ratio [–]
s	area [μm^2]
x	mesh size [μm]
Y	yield [–]

Subscripts:

i	the index of the fraction
j	the index of the subfraction

Demineralization behavior of bovine bone granules

3.1 Introduction

In this chapter, bovine bone granules are demineralized in nitric acid. The calcium concentration in the solution is measured at a given time. The demineralization behavior is characterized by fitting to a first order equation according to the rate equation stated in Chapter 1. This treatment is modified based on the particulate properties obtained in Chapter 2. The demineralization rate is discussed with considering the particulate properties.

3.2 Experimental procedure

3.2.1 Demineralization

A bovine bone block was pulverized for 60 s or 120 s at a revolution speed of 8000 rpm by the same way described in Chapter 2 and classified with sieves of 500, 710, 1000, and 2000 μm. Fifty milligrams of the granule of each fraction was put into 50 mL of 2% nitric acid and kept at 303 K with a thermostatic shaker reciprocating at 130 rpm with a stroke of 3 cm. The solution was drawn at given intervals as 0.5 h, 1 h, 2 h, 4 h and 24 h. Then, the bone granules demineralized, i.e. DBM, was filtered, washed, and freeze-dried. Part of the dry DBM was ground with a mortar and a pestle, and it was demineralized again for 24 h to evaluate calcium content remained in the DBM.

3.2.2 Characterization

The morphology of the bone granules was observed under an optical microscope and analyzed with image analysis software, ImageJ. The characteristic lengths *a* and *b* were defined as in Chapter 2. The aspect ratio of lengths *a* and *b* is expressed as $r_{ab} = \frac{a}{b}$ in this chapter.

The characteristic diameter *d* was obtained as an equivalent circle diameter from

$$\frac{\pi}{4}ab = \frac{\pi}{4}d^2 . \tag{3-1}$$

Some granules were put on a double-sided tape stuck on a slide glass plate and observed from the horizontal direction to measure the height *c*. Another aspect ratio r_{ac} was defined as

$$r_{ac} = \frac{a}{c} . \tag{3-2}$$

The density ρ was measured with a densimeter. The elemental analysis was performed with an electron probe microanalyzer (EPMA) to examine the characteristic X-ray image of CaKα. The calcium concentration in the solution was measured by inductivity coupled plasma-atomic emission spectroscopy (ICP-AES).

The degree of demineralization was evaluated by the normalized calcium content α defined as

$$\alpha = \frac{\omega}{\omega_0} ,$$

where ω is the amount of substance of calcium can be expressed as

$$\omega = (C_\infty + C_{\mathrm{g},\infty} - C)V$$

and ω_0 is that before demineralization can be expressed as

$$\omega_0 = (C_\infty + C_{g,\infty})V$$

This equation can be rewritten as

$$\alpha = \frac{C_\infty + C_{g,\infty} - C}{C_\infty + C_{g,\infty}} \tag{3-3}$$

where C is the calcium concentration in the solution, C_∞ is the calcium concentration in solution for 24 h, and $C_{g,\infty}$ is the equivalent concentration of calcium which equals the calcium content remained in bone granules per volume of solution demineralized for 24 h. The numerator of this equation is represented for the calcium content in DBM, and the denominator is for the total calcium content in original bone granules. This value ranges from 1 to 0, which corresponds to 0 to 100 % of the degree of demineralization. For evaluating the dispersion of an arbitrary amount X, the coefficient of variance CV(X) was calculated by using the standard deviation SD(X) and the average Av(X) as

$$\mathrm{CV}(X) = \frac{\mathrm{SD}(X)}{\mathrm{Av}(X)}.$$

3.3 Results and discussion

3.3.1 Demineralization behavior

Fig. 3-1 shows the change in the calcium concentration C in the solution with demineralizing time t. For Fraction I of the specimen pulverized for 60 s, C was 0.73×10^{-4} mol/L for a demineralizing time of 0.5 h, and it was monotonically increased to 0.93×10^{-4} mol/L for 1 h and to 1.31×10^{-4} mol/L for 24 h. The value of C was lower for coarser fractions. The specimens pulverized for 120 s were dissolved

more than for 60 s.

The calcium content remained in DBM was evaluated, and $C_{g,\infty}$ was confirmed as zero. It indicated the DBM reached the complete demineralization at 24 h. Based on this result and the value shown in Fig. 3-1, the normalized calcium content α was obtained, and its change with the demineralizing time t was illustrated in Fig. 3-2. This figure demonstrates the progress of demineralization. For the specimens obtained for a pulverizing time of 60 s, α of Fraction I was 0.34 for a demineralizing time of 0.5 h and 0.008 for 4 h and it decreased to zero for 24 h. This tendency was the same for the other fractions. It was confirmed that the mass balance of calcium amount dissolved in the solution and remained in the DBM has been achieved at any demineralizing time.

Fig. 3-3 depicts the results of mapping analysis of CaKα by EPMA. For a bone granule shown in Fig. 3-3A, calcium was distributed over the whole granule. The bright regions in which calcium was detected were reduced by demineralization for 1 h, as shown in Fig. 3-3B. Fig. 3-3C shows that calcium was not apparently detected on the surface of the granule demineralized for 4 h, which indicated the minerals on the surface were demineralized into the solution. Thus, it is confirmed that the specimen demineralized for 1 h was in partially demineralized state.

The initial demineralization rate was the fastest for Fraction I and the slowest for Fraction III, as shown in Fig. 3-2. This may be understood intuitively that it is due to the difference in particle size. Fig. 3-4 illustrates the dependence of the average particle size D on the normalized calcium content α in DBM demineralized for 1 h.

Altogether, a positive correlation between them may be recognized, but it is very weak. This means that although smaller granules are demineralized faster, there should be another factor as well. In Chapter 2, it was described that a fraction with the same particle size can have a different aspect ratio. To confirm the effect of the aspect ratio on demineralization, the relationship between the normalized calcium content α in DBM demineralized for 1 h and the average aspect ratio R from r_{ab} was demonstrated in Fig. 3-5. All specimens of Fractions II have almost the same D around 1200 μm as seen in Fig. 3-4 but different R. A negative correlation between R and α is totally recognized, of which a correlation coefficient is −0.80, as expected. The same thing can be concluded for Fraction I, but the correlation was very weak as indicating by a correlation coefficient of −0.36. Consequently, it was concluded that another approach is necessary to characterize the demineralization behavior.

3.3.2 Kinetics of demineralization

As shown in Fig. 3-1, the calcium concentration C in the solution was increased toward the complete demineralization of calcium in bone granules with increasing demineralizing time t. This tendency has been expressed for the demineralization of bone by a researcher [Castro-Ceseña et al., 2011] as

$$\frac{\mathrm{d}C}{\mathrm{d}t} = k(C_\infty - C), \tag{3-4}$$

where k is a rate constant. This equation represents the demineralization of bone granules to be a first order process. Substituting Eq. (3-3) into Eq. (3-4), the rate equation can be expressed by using α as

$$\frac{\mathrm{d}\alpha}{\mathrm{d}t} = -k\alpha \ . \tag{3-5}$$

The integration of this equation gives

$$\ln\alpha = -k\,t\,. \tag{r1}$$

Fig. 3-5 was drawn by fitting the data to Eq. (r1). A linear relationship is recognized for each fraction. It may be confirmed that the demineralization rate $\mathrm{d}\alpha/\mathrm{d}t$ is proportional to α. However, the slope is different from fraction to fraction. Since this slope corresponds to the rate constant k, it should be essentially of one value for the present system. This result suggests that there is another factor to be considered.

Demineralization is the dissolution of the mineral component in an acid, which is a phenomenon at the solid surface. Therefore, it should be considered that the demineralization rate is proportional to the surface area. Incorporating this consideration, Eq. (3-5) can be rewritten as

$$\frac{\mathrm{d}\alpha}{\mathrm{d}t} = -k\,S\,\alpha\,, \tag{3-6}$$

where S is the specific surface area. If S is regarded to be constant, this equation can be integrated to give

$$\ln\alpha = -k\,S\,t\,. \tag{r2}$$

As well known, a volume-based specific surface area can be estimated as

$$S = \frac{\phi}{d}\,, \tag{3-7}$$

where ϕ is a shape factor. Through the application of the equivalent circle to each granule, d is adoptable as the circle equivalent diameter. However, the actual shape of the granules is irregular. Now, we suppose that the granule is an oblate ellipsoid, and the morphology is characterized by three lengths a, b and c. It is easy to measure the

lengths a and b of all granules by regarding the shape to be elliptic and to determine the equivalent circle diameter d as the characteristic size, which is defined as Eq. (3-1). However, it is not so convenient to measure the length c for all granules at the same time. For ease of operation, it is desirable to adopt one characteristic value with respect to the length c.

Table 3-1 lists the average and standard deviation of the length c and the aspect ratio r_{ac} for each fraction. The Av(c) values are not concerned with the mesh size of the sieves used, because the decisive length for sieving is the only b. However, the CV(c) values are similar to each other, suggesting that there may be a certain tendency. The CV(c) and CV(r_{ac}) for Fraction I were 0.36 and 0.28, respectively. Also for the other fractions, the CV(r_{ac}) was smaller than CV(c). Hence, I decided to adopt r_{ac} as a characteristic coefficient to express c as

$$c = a\, r_{ac}^{-1} \tag{3-8}$$

for individual granules.

The volume V of an oblate ellipsoid is

$$V = \frac{\pi}{6} abc = \frac{\pi}{6} d_{\mathrm{e}}^{3},$$

where d_{e} is an equivalent sphere diameter, that is

$$d_{\mathrm{e}} = \sqrt[3]{abc}\,. \tag{3-9}$$

Since the aspect ratio of a to b is defined as Eq. (2-7), b can be expressed as

$$b = a\, r_{ab}^{-1}. \tag{3-10}$$

Substituting Eq. (3-10) into Eq. (3-1), a can be expressed as a function of d:

$$a = d\, r_{ab}^{\frac{1}{2}}. \tag{3-11}$$

Substituting Eqs. (3-8), (3-10), and (3-11) into Eq. (3-9), d_e can be expressed as

$$d_e = \sqrt[3]{\left(d\, r_{ab}^{\frac{1}{2}}\right)\left(d\, r_{ab}^{\frac{1}{2}}\, r_{ab}^{-1}\right)\left(d\, r_{ab}^{\frac{1}{2}}\, r_{ac}^{-1}\right)} = d\, r_{ab}^{\frac{1}{6}}\, r_{ac}^{-\frac{1}{3}}. \tag{3-12}$$

Substituting d_e in Eq. (3-12) into d in Eq. (3-7), the shape factor of an elliptic granule is expressed as

$$\phi = 6 r_{ab}^{-\frac{1}{6}} r_{ac}^{\frac{1}{3}}. \tag{3-13}$$

The values ϕ and S of the specimens are calculated and list in Table 3-2. Fig. 3-7 is the result of approximation according to Eq. (r2). All fractions are shown to be in linear relationship again, and the values of the slope became much closer. From this result, it may be confirmed that the surface area is constant during demineralization.

Fig. 3-8 illustrates the optical micrographs of a bone granule before and after demineralization. With increasing the demineralizing time, the translucency was increased. This depicts that the mineral component was dissolved out as the demineralization went on. The shape and size seem almost unchanged during demineralization. Therefore, the effective surface area can be regarded to be of outer surface of the granule, which is characterized in the initial state before demineralization.

The slopes of the lines drawn in Fig.3-7 became closer as stated above, but they are still different from each other. To improve the accuracy, more modification will be attempted.

The specific surface area obtained by calculation is the apparent external surface area. It should be considered that demineralization does not occur on the whole surface of the granule but just the mineral phase. The effective specific surface area is

estimated by multiplying S by the surface area ratio of the mineral component to the whole granule. Suppose that sufficiently tiny domains of the mineral component are distributed homogeneously in a granule, the surface area ratio can be equated with the volume ratio

$$\theta = \frac{V_{\mathrm{M}}}{V} . \tag{3-14}$$

The volumes of the mineral component, the protein component and the whole granule are expressed by each mass m and density ρ as

$$V_{\mathrm{M}} = \frac{m_{\mathrm{M}}}{\rho_{\mathrm{M}}}, \quad V_{\mathrm{P}} = \frac{m_{\mathrm{P}}}{\rho_{\mathrm{P}}}, \text{ and } \quad V = \frac{m}{\rho},$$

where the subscripts M and P designate the mineral component and protein phase, respectively. Since $V = V_{\mathrm{M}} + V_{\mathrm{P}}$, Eq. (3-14) is rewritten as

$$\theta = \frac{\rho - \rho_{\mathrm{P}}}{\rho_{\mathrm{M}} - \rho_{\mathrm{P}}} .$$

Finally, a modified rate equation is obtained as

$$\frac{\mathrm{d}\alpha}{\mathrm{d}t} = -k\,\theta S\,\alpha .$$

Integrating the modified rate equation to give

$$\ln \alpha = -k\,\theta S\,t . \tag{r3}$$

For calculating θ, the density having been measured for the granules to be demineralized was used as ρ, and 3.15 g/cm^3 of calcium-deficient hydroxyapatite [Wilson et al., 2005] and 1.35 g/cm^3 of protein [Heidemann and Rieß, 1964] were used as ρ_{M} and ρ_{P}, respectively. The measured density and calculated surface area ratio are listed in Table 3-3. The result according to Eq. (r3) is illustrated in Fig. 3-10. The slope of all lines became still closer, and therefore it can be seen that the

procedure proposed above is appropriate.

In order to discuss the accuracy of the treatments described above, the dispersion of the rate constant k will be compared. Since the dimension of k in Eqs. (r1) to (r3) is not the same as each other, it is not proper to compare them directly. Therefore, k was normalized to be

$$K = \frac{k}{\mathrm{Av}(k)},$$

where Av(k) is the average of k for each equation. It is found that the normalized rate constant K was converged to unity from Eqs. (r1) to (r3), as illustrated in Fig. 3-11(A). To quantify the extent of dispersion, CV(K) was calculated and plotted in Fig. 3-11(B). The CV(K) value for Eq. (r3) was 0.021, whereas 0.09 for Eq. (r2). Although the accuracy was increased a little from sphere to ellipsoid model, Eq. (r3) gives the most precise approximation, so that the approximate lines can be regarded as almost one line. It is expected that the treatment according to Eq. (r3) can be used for predicting how much demineralizing time would be necessary to obtain DBM with a desirable degree of demineralization.

As described in Section 3.3.1, it is insufficient to discuss the demineralization behavior just with respect to the granule size. In this section, it was stated that the treatment involving the surface area can provide a successful result. The surface area of powdery specimens is commonly measured by nitrogen adsorption, or the BET method. This is an established technique, very popular with and familiar to chemists and engineers. This method has been used for characterization of bone [Lurtwitayapont and Srisatit, 2010]. However, this method is confirmed that it is not

so convenient. Low molecular weight components, e. g. water which the bone granules contain, should be removed by a pre-treatment such as heating at around 573 K. If the specimen is heated excessively, the protein phase would be denatured. The operator should have the certain skills to perform it well. The value to be measured is the total surface area including the protein phase and is not consistent with that of the mineral component to be dissolved. The measuring instrument is expensive, and therefore not all clinics can install it. The treatment proposed in this study provides an alternative, convenient manner, which would be available in any clinic.

3.4 Conclusions

Bovine bone granules were dissolved in nitric acid, and the demineralization behavior was characterized to determine how the appropriate conditions for preparing DBM would be found. It was tried to relate the calcium content to the granule size or aspect ratio. Weak correlations between them were recognized, but they were not sufficient to discuss the demineralization behavior. The change in the calcium content with the demineralization time was fitted to a first order rate equation. The treatment was modified by regarding the shape of granules to be ellipsoidal and by expressing the contribution of the effective surface area with the density measured. This procedure is advantageous in terms that it does not demand any special, expensive equipment. I expect that doctors, dentists, and researchers in this area will apply the treatment proposed in this study to the preparation of DBM.

Figures and tables:

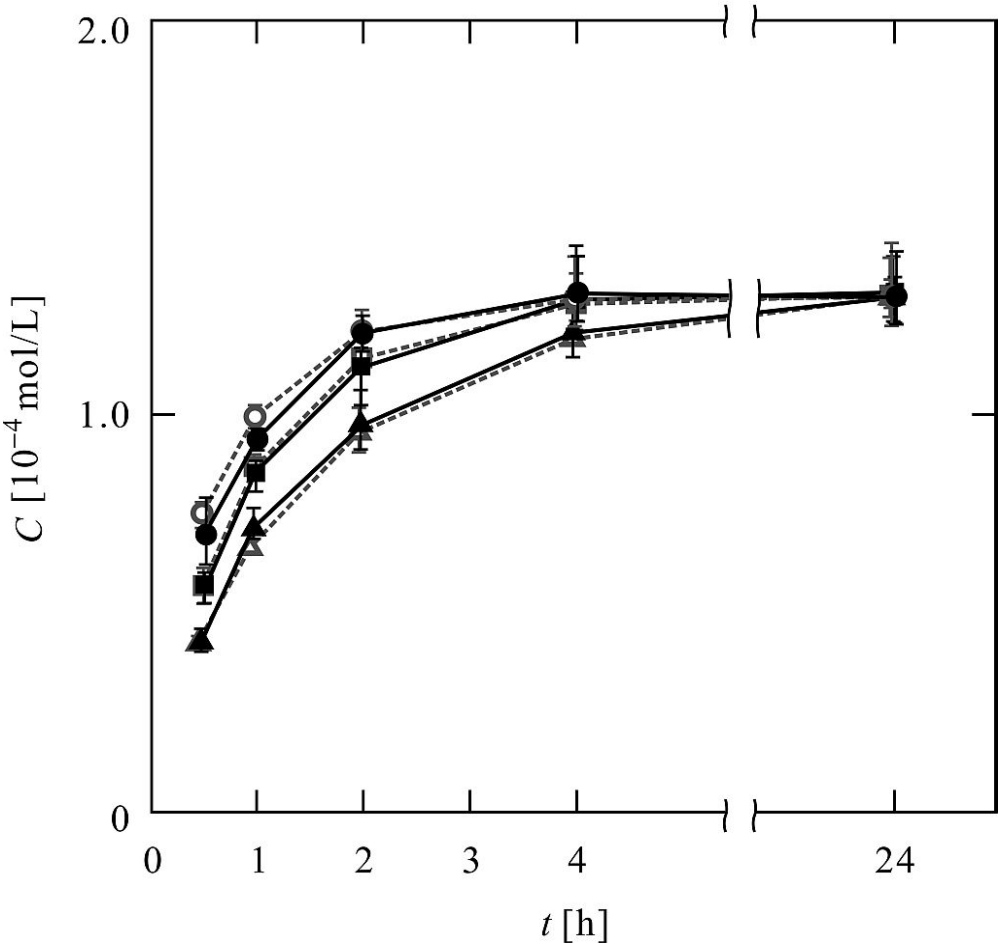

Fig. 3-1. Change in the calcium concentration in the solution with demineralizing time. Pulverizing time: (■) 60 s, (□) 120 s. ●: Fraction I, ■: Fraction II, ▲: Fraction III.

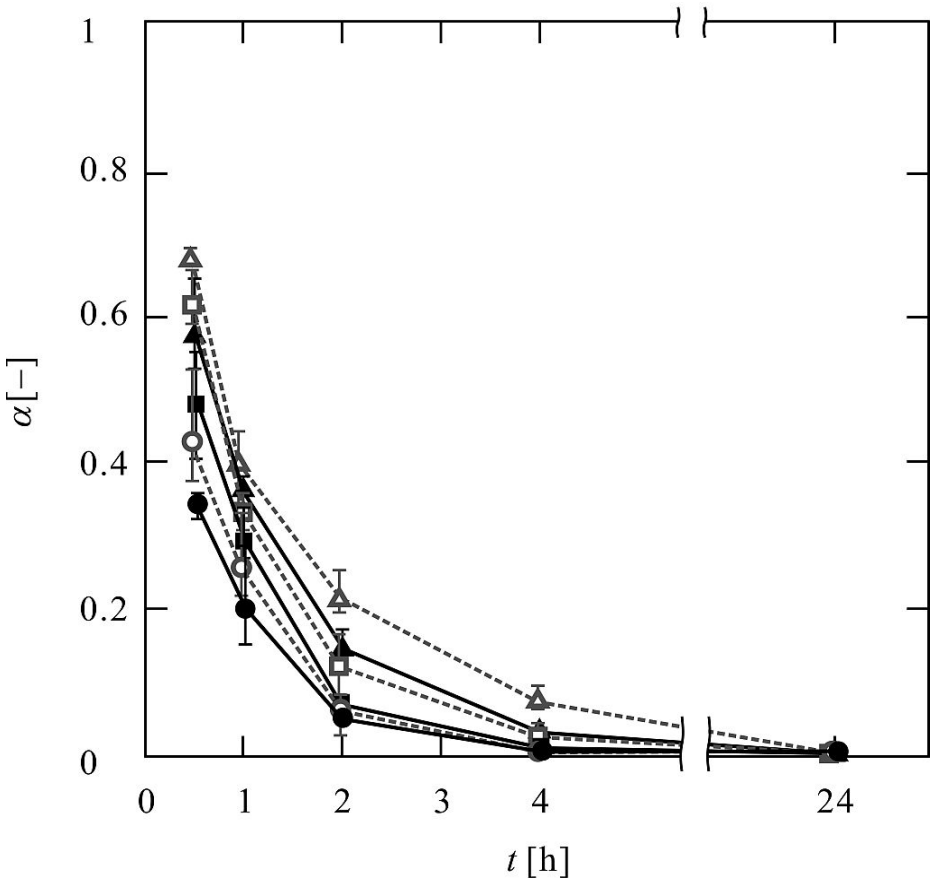

Fig. 3-2. Change in the calcium content in the DBM with demineralizing time. Pulverizing time: (■) 60 s, (□) 120 s. ●: Fraction I, ■: Fraction II, ▲: Fraction III.

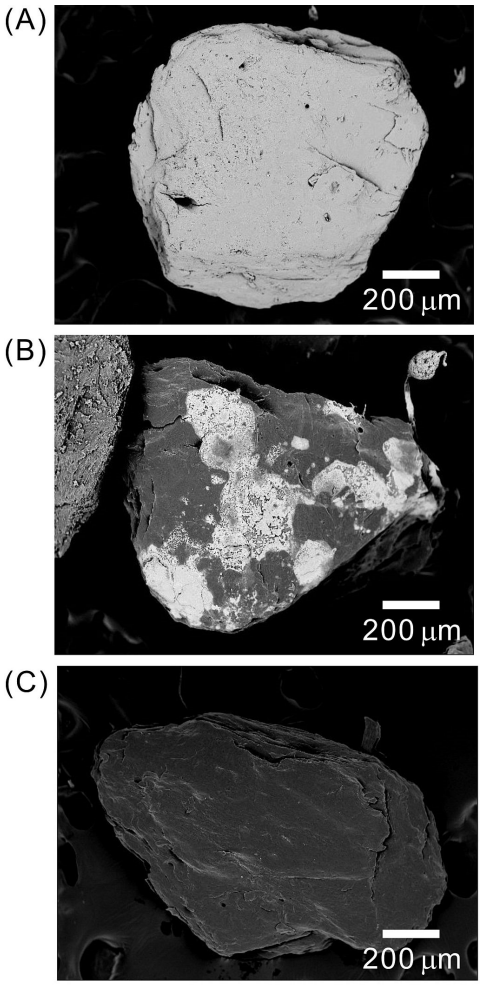

Fig. 3-3. X-ray images of CaKα of a granule in Fraction II obtained for a pulverizing time of 60 s. (A) Bone granule, and DBMs demineralized for (B) 1 h and (C) 4 h.

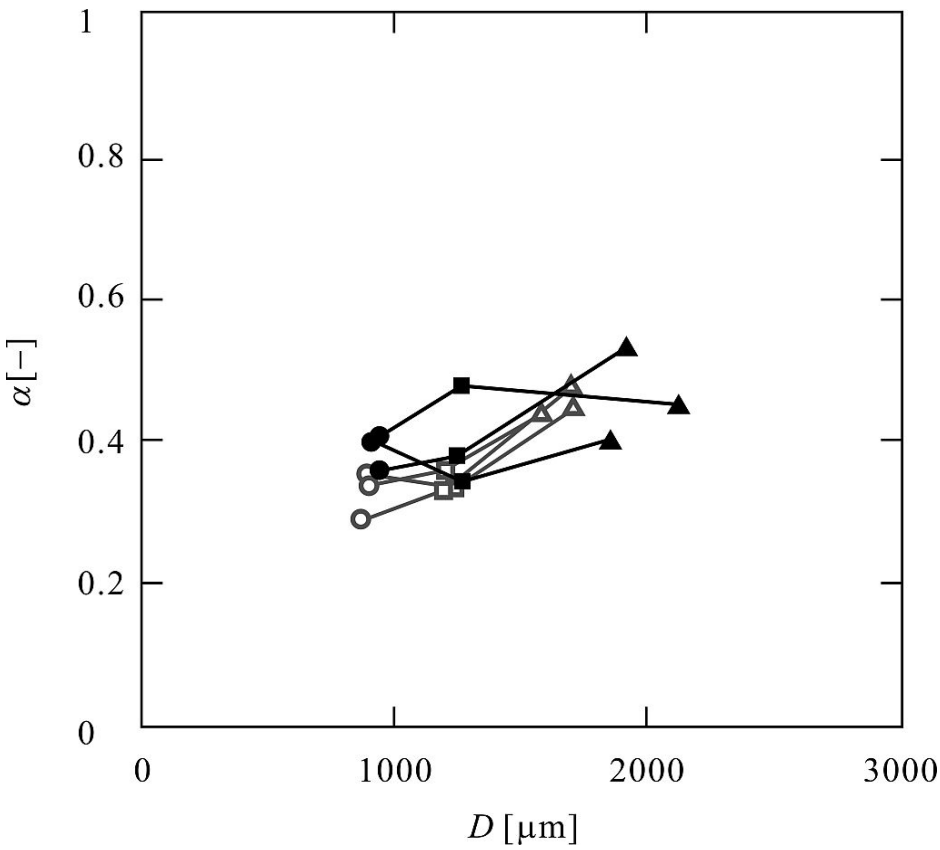

Fig. 3-4. Relationship between the calcium content in the DBM demineralized for 1 h and the average particle size of bone granules. Pulverizing time: (■) 60 s, (□) 120 s. ●: Fraction I, ■: Fraction II, ▲: Fraction III.

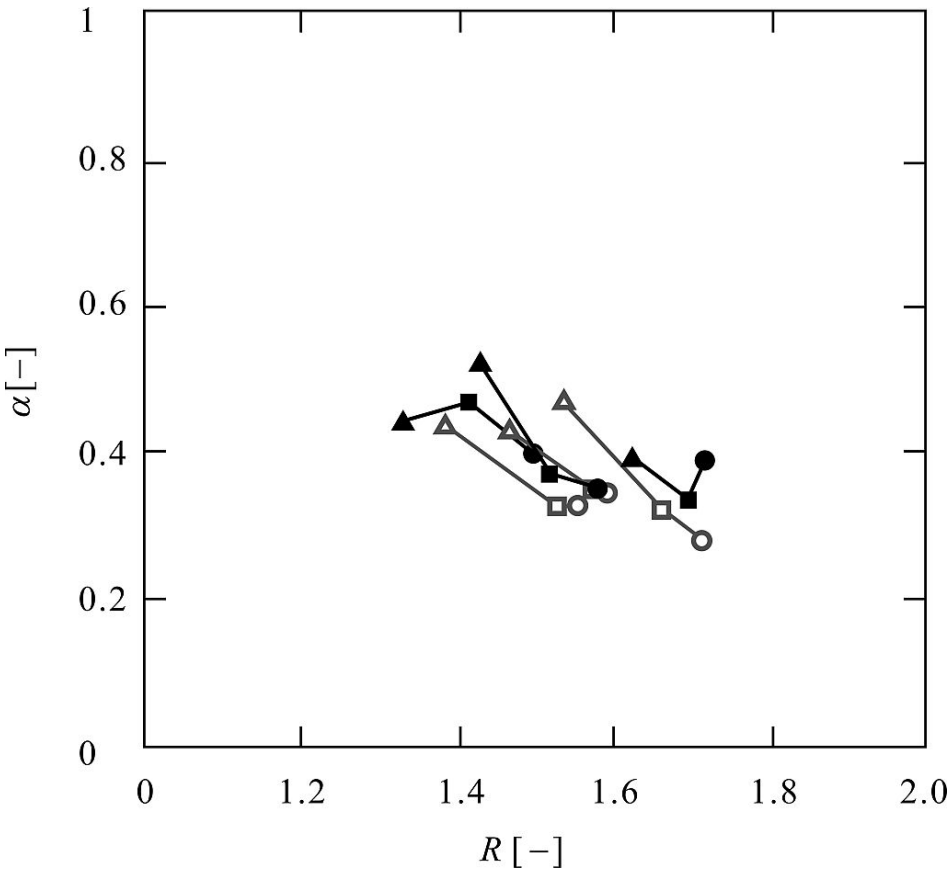

Fig. 3-5. Relationship between the calcium content in the DBM demineralized for 1 h and the average aspect ratio of lengths *a* to *b* of bone granules. Pulverizing time: (■) 60 s, (□) 120 s. ●: Fraction I, ■: Fraction II, ▲: Fraction III.

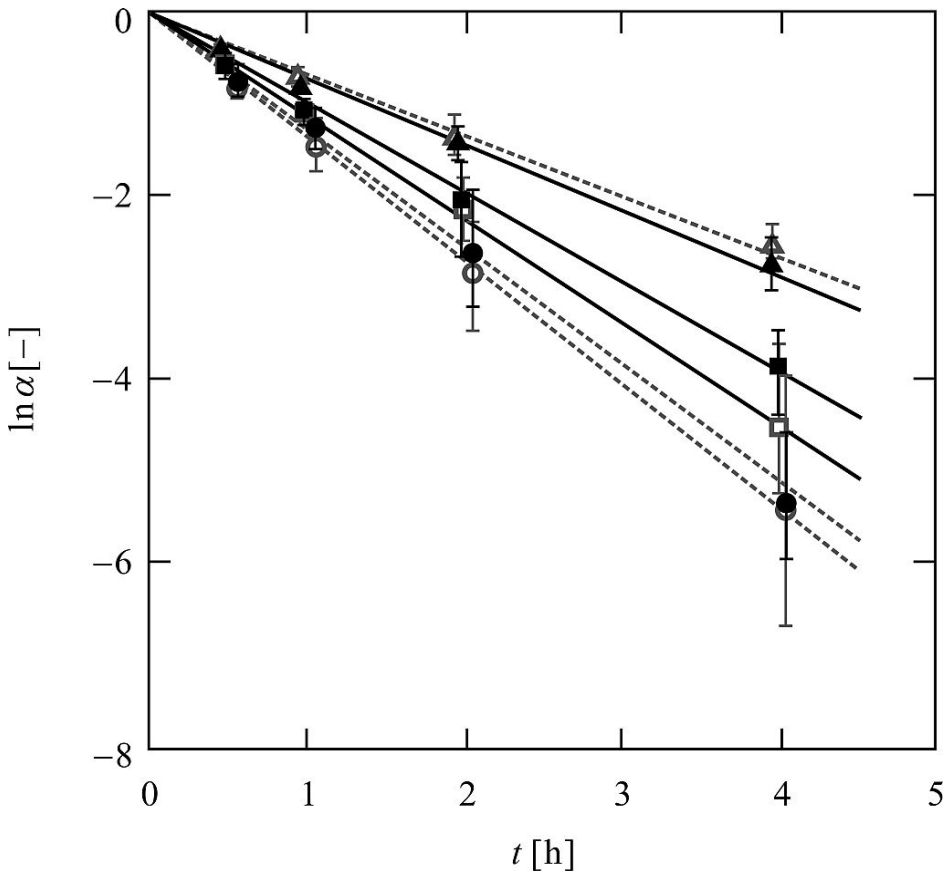

Fig. 3-6. Analysis according to the integrated rate equation (r1). Pulverizing time: (■) 60 s, (□) 120 s. ●: Fraction I, ■: Fraction II, ▲: Fraction III.

Table 3-1. The average, standard deviation, and coefficient of variance of the length *c* and aspect ratio of *a* to *c* of the specimens obtained for a pulverizing time of 60 s.

Fraction	Length *c*			Aspect ratio r_{ac}		
	Av [μm]	SD [μm]	CV [–]	Av [–]	SD [–]	CV [–]
I	266	97	0.36	2.7	0.76	0.28
II	331	125	0.38	3.0	0.95	0.32
III	432	157	0.36	3.1	0.89	0.29

Av: average, SD: standard deviation, CV: coefficient of variance

Table 3-2. The normalized shape factor, specific surface area and the normalized specific surface area of the specimens obtained for a pulverizing time of 60 and 120 s.

Fraction		ϕ [−]		S [10^{-2} μm^{-1}]	
	No.	60 s	120 s	60 s	120 s
	1	7.731	7.850	8.453	8.747
I	2	7.731	7.806	8.225	8.776
	3	7.765	7.840	9.355	9.068
	1	7.787	7.880	6.448	6.706
II	2	7.731	7.865	6.240	5.909
	3	7.872	7.885	6.318	5.858
	1	7.817	7.984	4.384	5.273
III	2	7.833	7.906	4.828	3.805
	3	7.927	7.942	4.294	3.643

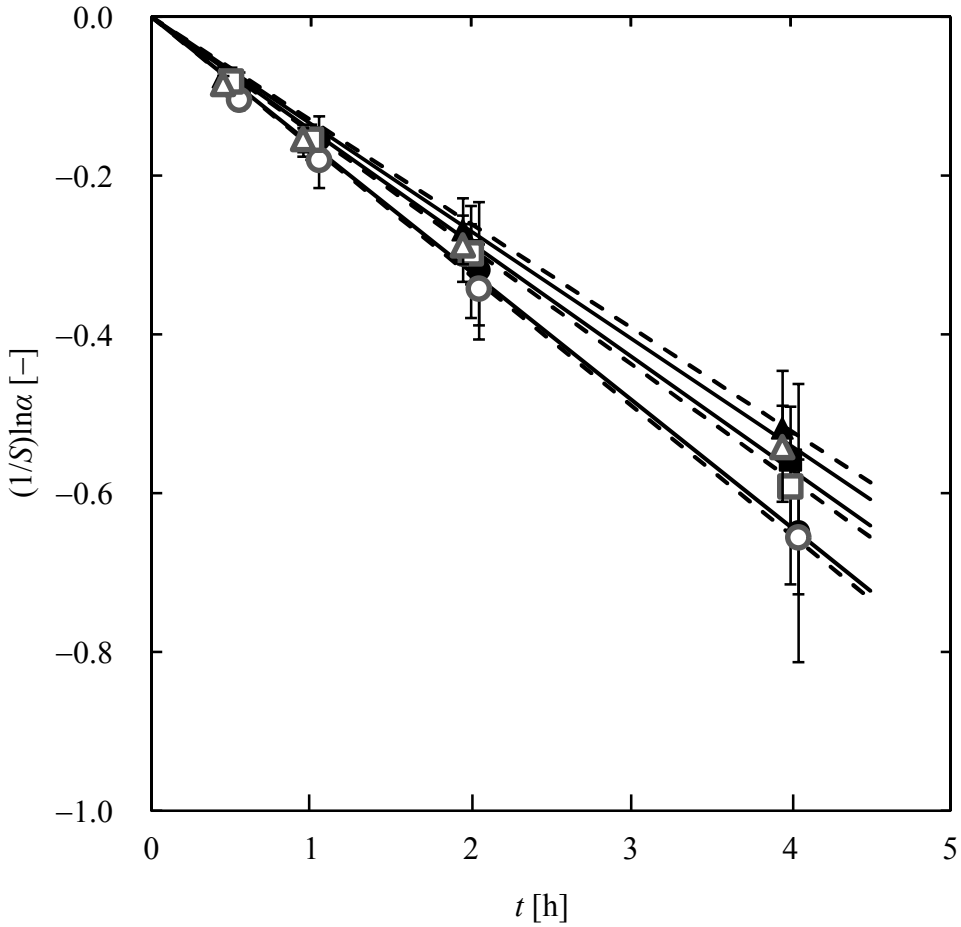

Fig. 3-7. Analysis according to the integrated rate equation (r2). Pulverizing time: (■) 60 s, (□) 120 s. ●: Fraction I, ■: Fraction II, ▲: Fraction III.

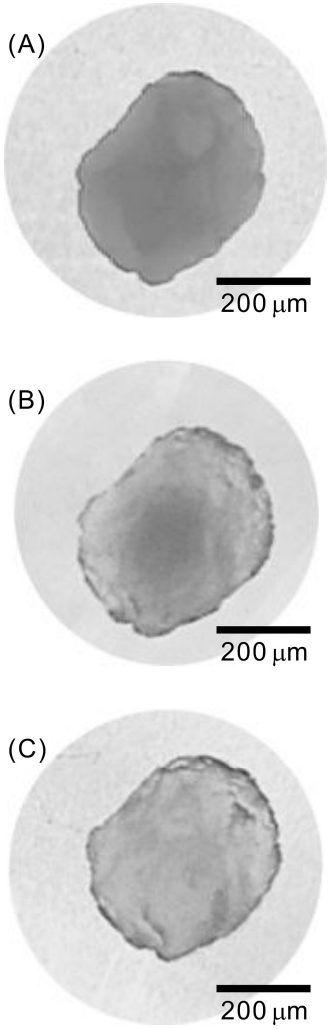

Fig. 3-8. Optical micrographs of a granule in Fraction II obtained for a pulverizing time of 60 s. (A) Bone granule, and DBMs demineralized for (B) 1 h and (C) 4 h.

Table 3-3. The density, surface area ratio and the effective surface area of the specimens obtained for a pulverizing time of 60 and 120 s.

Fraction		ρ [g/cm^3]		θ [–]		θS [10^{-2} /μm]	
	No.	60 s	120 s	60 s	120 s	60 s	120 s
	1	2.270	2.580	0.618	0.822	5.228	7.193
I	2	2.390	2.430	0.697	0.724	5.736	6.351
	3	2.510	2.460	0.776	0.743	7.263	6.741
	1	2.270	2.40	0.618	0.704	3.988	4.721
II	2	2.250	2.340	0.605	0.664	3.777	3.926
	3	2.180	2.30	0.559	0.638	3.533	3.738
	1	2.160	2.190	0.546	0.566	2.394	2.984
III	2	2.110	2.220	0.513	0.586	2.477	2.228
	3	2.080	2.120	0.493	0.520	2.119	1.894

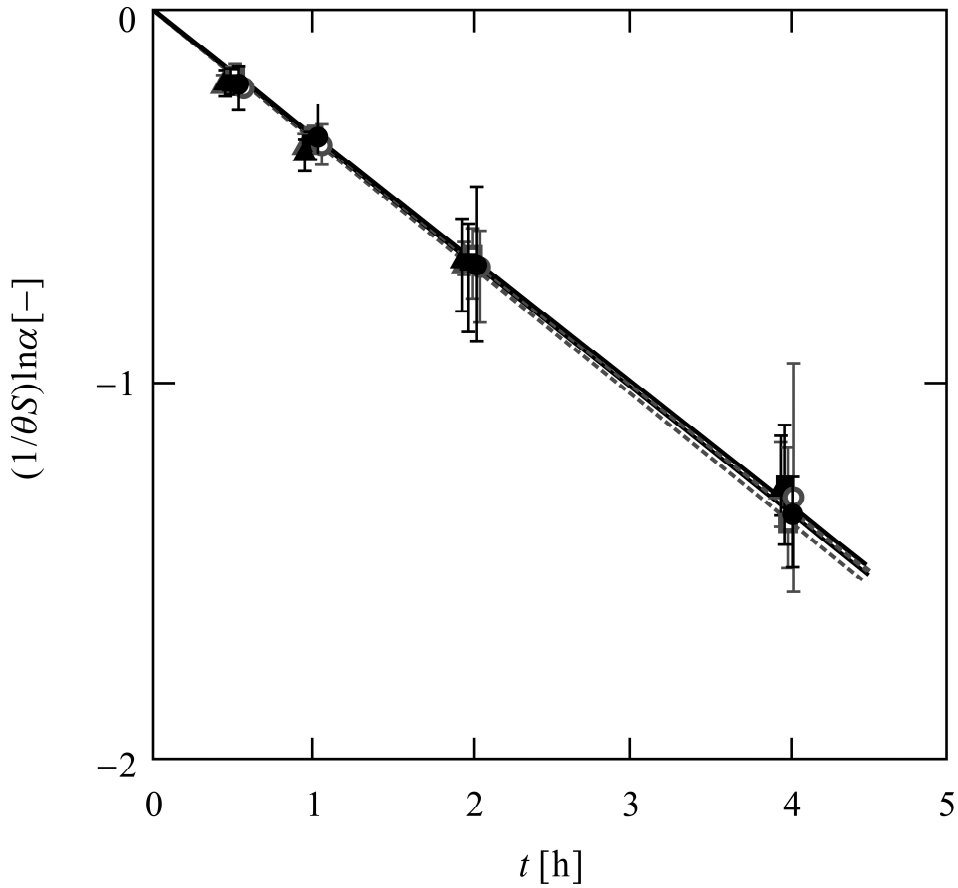

Fig. 3-9. Analysis according to the integrated rate equation (r3). Pulverizing time: (■) 60 s, (□) 120 s. ●: Fraction I, ■: Fraction II, ▲: Fraction III.

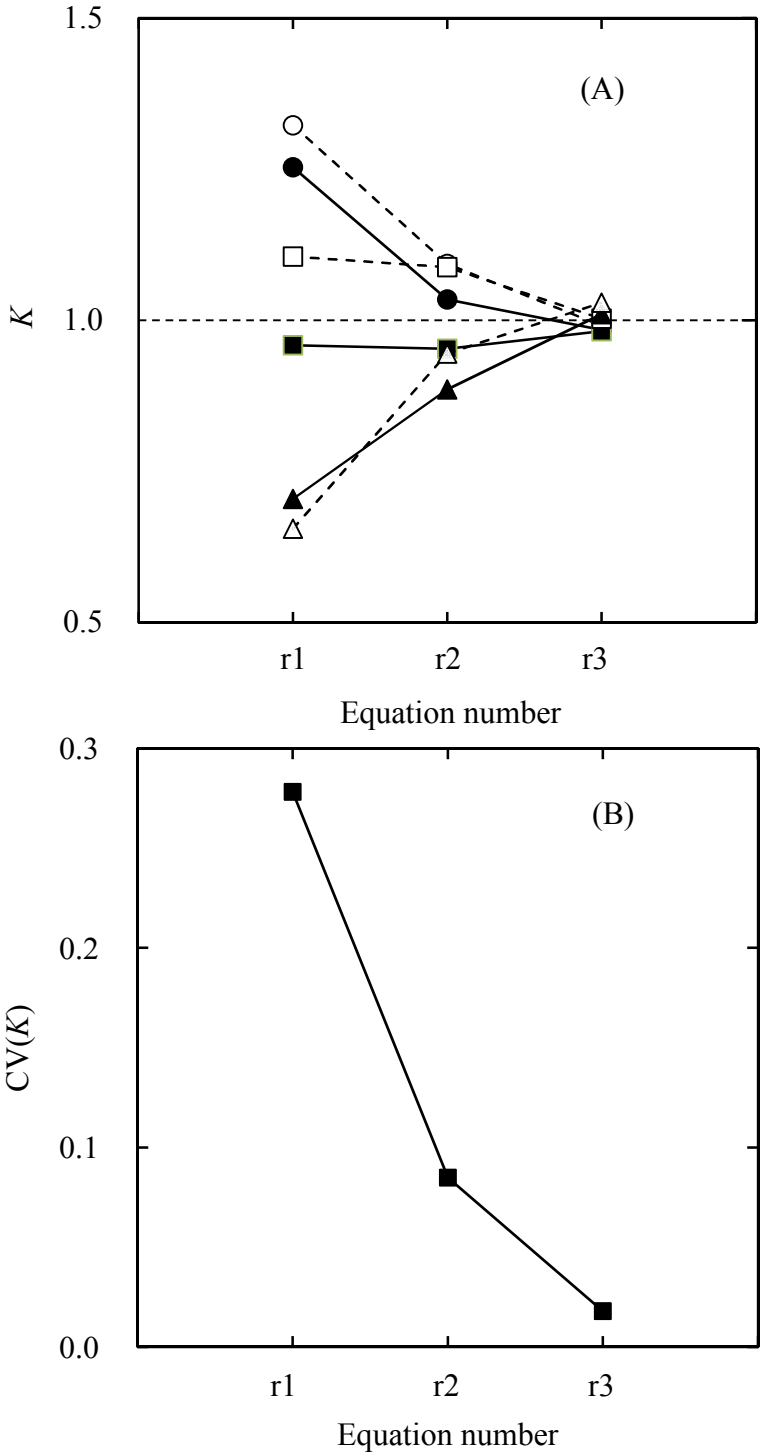

Fig. 3-10. Comparison of the normalized rate constant and the coefficient of variance according to the integrated rate equations (r1) to (r3). Pulverizing time: (■) 60 s, (□) 120 s. ●: Fraction I, ■: Fraction II, ▲: Fraction III..

Nomenclature

a	length [μm]
Av(X)	average of X
b	length [μm]
c	length [μm]
C	calcium concentration [mol/L]
CV(X)	coefficient of variance for X [–]
d	characteristic diameter [μm]
D	average particle size [μm]
d_e	equivalent sphere diameter [μm]
k	rate constant
K	normalized rate constant [–]
m	mass [g]
r	aspect ratio [–]
R	average aspect ratio [–]
S	specific surface area [μm^{-1}]
SD(X)	standard deviation of X
t	demineralizing time [h]
V	volume of a granule [cm^3]
X	arbitrary amount
α	normalized calcium content [–]
ϕ	modified shape factor [–]

θ volume ratio [–]

ρ ensity [g/cm^3]

ω amount of substance of calcium [mol]

subscript

0 before demineralization

g granule

M mineral

P protein

∞ complete demineralization

General conclusions

The study of this thesis was carried out as a fundamental study for preparing DBM, which is used for bone regeneration in regenerative medicine.

In Chapter 1, the background of bone regeneration with DBM was explained. There are a lot of reports successful in promoting bone regeneration. However, the optimum size range of DBM reported on osteoinduction is scattered and has not been fixed yet. I thought that one of reasons may be because of the uncertainty in the characterization of particulate properties such as the particle size, size distribution, and aspect ratio, etc. These particulate properties may effect on the demineralization behavior. The objectives of this thesis were set as to characterize the particulate properties of bone granules and to characterize their demineralization behavior.

In Chapter 2, bovine bone was pulverized with a high-speed blade mill, and the size of each granule after sieving was measured by image analysis. A new method to express the particle size distribution was proposed by combining the results from both sieving and image analysis. It was found that there was a negative correlation between the average aspect ratio and average particle size. The granules having the same average particle size revealed different aspect ratio. From these results, it was anticipated that the demineralization behavior would be related to such particulate properties.

In Chapter 3, bovine bone granules were demineralized in nitric acid, and the

demineralization behavior was discussed. The change in the normalized calcium content with the demineralizing time was fitted to a first order rate equation. The specific surface area in this equation was calculated from the results of the particulate properties characterized in Chapter 2. The fitting of data to the rate equation was improved by regarding the contribution of the effective surface area of the mineral phase.

When doctors and dentists carry out the treatments for bone regeneration with DBM, it is necessary to prepare DBM with the same degree of demineralization. It is expected that the results of this study is helpful for determining the demineralization conditions according to the particulate properties of bone granules to be used. For example, if the supply of DBM with a certain degree of demineralization is requested, the average size, aspect ratios, and density are characterized for each fraction obtained by sieving, and then it can be suggested how long the demineralization should be conducted.

References:

Akazawa T., Murata M., Tazaki J., Hino J., Nakamura K., Yoshinari S., Tabata Y., Hanawa T., Takahata M., Iwasaki N., Ito M., Ohamori T., Tamachika H., Kikuchi M., 2012a. “Characterization of bio-absorble and biomimetic granules produced from animal bone by the high velocity rotation-crushing and demineralizaing technique”. Phosphorus Research Bulletin. 26: 65−70.

Akazawa T., Murata M., Minamida Y., Wei T., Arafat K., Hino J., Tazaki J., Ito M. and Kimura I., 2012b. "Bioactive surface structure and bio-absorption of human dentin granules designed by the supersonic demineralization and biomimetic coating technique". Journal of Hard Tissue Biology. 21: 351–358.

Allen T., 2003. “Particle size analysis by sieving” in Powder sampling and particle size determination. Elsevier Science. pp.208–250.

Bates P., Ramachandran M., 2007. “Bone injury, healing and grafting” in Basic Orthopaedic Sciences. The Stanmore Guide. Edited by Ramachandran M., Hodder Arnold. Stanmore. pp.123–134.

Birkedal-Hansen H., 1974a. “Diffusion of $H^{36}Cl$ in decalcified ivory dentine”. Journal of Histochemistry & Cytochemistry. 22: 428–433.

Birkedal-Hansen H., 1974b. “Kinetics of acid demineralization in histologic technique”. Journal of Histochemistry & Cytochemistry. 22: 434–441.

Black D.L., McQuay M.Q., Bonin M.P., 1996. “Laser-based techniques for particle-size measurement: A review of sizing methods and their industrial applications”. Progress in Energy and Combustion Science. 22: 267–306.

Castro-Ceseña A.B., Novitskaya E.E., Chen P.Y., Hirata G.A., McKittrick J., 2011. “Kinetic studies of bone demineralization at different HCl concentrations and temperatures”. Materials Science and Engineering C. 31: 523–530.

Chalmers J., Sissons H.A., 1959. “An experimental comparison of bone-grafting materials in the dogs”. The Journal of Bone and Joint Surgery. 41-B: 209.

Compston J.E., 2001. “Sex steroids and bone”. Physiological review. 81:419–447.

Cruvinel P. E., Vieira S. R., Crestana S., Minatel E. R., Mucheroni M. L., Neto A. T., 1999. “Image processing in automated measurements of raindrop size and distribution”. Computers and Electronics in Agriculture. 23: 205–217.

Gepstein R., Weiss R.E., Hallel T., 1987. “Bridging large defects in bone by demineralized bone matrix in the form of a powder”. The Journal of Bone and Joint Surgery. 69A: 984–992.

Glowacki J., Murray J.E., Kaban L.B., Folkman J., 1981a. “Application of the biological principle of induced osteogenesis for craniofacial defects”. The Lancet. 317: 959–962.

Glowacki J., Altobelli D., Mulliken J.B., 1981b. “Fate of mineralized and demineralized osseous implants in cranial defects”. Calcified Tissue International. 33: 71–76.

Han B., Tang B., Nimni M.E., 2003. “Quantitative and sensitive in vitro assay for osteoinductive activity of demineralized bone matrix”. Journal of Orthopaedic Research. 21: 648–654.

Heidemann E., Rieß W., 1964. “Die Veränderungen des Kollagens bei Entwässerung mit Aceton und die Konsequenzen dieser Veränderung für die Kollagenstruktur”. Hoppe-Seyler's Zeitschrift für physiologische Chemie. 337: 101–113.

Igathinathane C., Pordesimo L.O., Batchelor W.D., 2009. “Major orthogonal dimensions measurement of food grains by machine vision using ImageJ”. Food Research International. 42: 76–84.

Igathinathane C., Pordesimo L.O., Columbus E.P., Batchelor W.D., Sokhansanj S., 2008. “Shape identification and particles size distribution from basic shape parameters using ImageJ”. Computers and Electronics in Agriculture. 68: 168–182.

Kaban L.B., Mulliken J.B., Glowaki J., 1983. “Treatment of jaw defects with demineralized bone implants”. Journal of Oral Maxillofac Surgery. 40: 623–626.

Kabir A.M., Murata M., Kusano K., Akazawa T., Shibata T., 2015. “Autogenous demineralized dentin graft for third molar socket regeneration – A case report”. Dentistry. 5: Doi:10.4172/2161-1122.1000343.

Kini U., Nandeesh B.N., 2013. “Physiological bases of bone regeneration II. The remodeling process” in Radionuclide and Hybrid Bone Imaging. Edited by Ignac F., Gopinath G., Van der Wall H., Springer. Berlin. pp.23–49.

Lees S., 1981. “A mixed packing model for bone collagen”. Calcified Tissue International. 33: 591–602.

Lewandrowski K.U., Venugopalan V., Tomford W.W., Schomacker K.T., Mankin H.J., Deutsch T.F., 1996. “Kinetics of cortical bone demineralization: controlled

demineralization–A new method for modifying cortical bone allografts". Journal of Biomedical Materials Research. 31: 365–372.

Lewandrowski K.U., Tomford W.W., Schomacker K.T., 1997. "Improved osteoinduction of cortical bone allografts: A study of the effects of laser perforation and partial demineralization". Journal of Orthopaedics Research. 15: 748–756.

Lurtwitayapont S., Srisatit T., 2010. "Comparison of lead removal by various types of swine bone adsorbents". Environment Asia. 3: 32–38.

Mazzoli A., Favoni O., 2012. "Particle size, size distribution and morphological evaluation of airborne dust particles of diverse woods by Scanning Electron Microscopy and image processing program". Powder Technology. 225: 65–71.

Murata M., Akazawa T., Takahata M., Ito M., Tazaki J., Hono J., Nakamura K., Iwasaki N., Shibata T. Alisue M., 2010. "Bone induction of human tooth and bone crushed by newly developed automatic mill". Journal of the Ceramic Society of Japan. 118: 434–437.

Novitskaya E., Castro-Ceseña A., Chen P.Y., Vasquez J., Urbaniak R., 2011. "Investigations into demineralized cortical bone". Materials Research Society Symposium Proceedings. 1301; DOI: 10.1557/opl.2011.195.

Sampath T.K., Reddi A.H., 1984. "Distribution of bone inductive proteins in mineralized and demineralized extracellular matrix". Biochemical Biophysical Research Communications. 119: 949–954.

Shapoff C.A., Bowers G.M., Levy B., Mellonig J.T., Yukna R.A., 1980. "The effect of

particle size on the osteogenic activity of composite grafts of allogeneic freeze-dried bone and autogenous marrow". Journal of Periodontology. 51: 625–631.

Sonis S.T., Kaban L.B., Glowacki J., 1983. "Clinical trial of demineralized bone powder in the treatment of periodontal defects". Journal of Oral Medicine. 38: 117–122.

Syftestad G., Urist M.R., 1979. "Degradation of bone matrix morphogenetic activity by pulverization". Clinical Orthopaedics and Related Research. 141: 281–285.

Tiedeman J.J., Connolly J.F., Strates B.S., Lipplello L., 1991. "Treatment of nonunion by percutaneous injection of bone marrow and demineralized bone matrix: An experimental study in dogs". Clinical Orthopaedics and Related Research. 268: 294–302.

Urist M.R., 1965. "Bone: Formation by autoinduction". Science. 698: 893–899.

Urist M.R., 1968a. "Surface-decalcified allogeneic bone (SDAB) implants. A preliminary report of 10 cases and 25 comparable operations with undecalcified lyophilized bone implants". Clinical Orthopaedics and Related Research. 56: 37–50.

Urist M.R., Dowell T.A., Hay P.H., Strates B.S., 1968b. "Inductive substrates for bone formation". Clinical Orthopaedics and Related Research. 59:59–96.

Urist M.R., Mclean F.C., 1952. "Osteogenetic potency and new-bone formation by induction in transplants to the anterior chamber of the eye". The Journal of Bone and Joint Surgery. 34-A: 443–475.

Wilson R.M., Elliott J.C., Dowker S.E.P., Rodriguez-Lorenzo L.M., 2005. “Rietveld refinements and spectroscopic studies of the structure of Ca-deficient apatite”. Biomaterials. 26: 1317–1327.

Zhang M., Powers R.M., Wolfinbarger L., 1997. “Effects of the demineralization process on the osteoinductivity of demineralized bone matrix”. Journal of Periodontology. 68: 1085–1091.

Acknowledgements

There are many people who have supposed and helped me during this time. First, I would like to express my deepest appreciation to Prof. Kimura, for guiding me into the fantastic world of micro powder, for helping me in many ways with his broad knowledge, wisdom, for supporting me when I was in a difficult situation.

Also, I am deeply grateful to Prof. Shimizu, Prof. Yamagiwa and Prof. Tanaka, for giving me useful advice and comments as members of my committee and for their full support to this project.

I cannot forget to thank Dr. Akazawa, who has sincerity and passion in science, for assistance in the whole project period, especially in the particulate characteristics study. Also I am thankful to Dr. Murata group who broaden my horizon to the field of dentine clinic.

The technical assistances of ICP analyzer from the Office for Environment and Safety and EPMA from Center for Instrumental Analysis of Niigata University are deeply acknowledged.

Also I really appreciated the interaction with our group members and colleagues for their helps and encouragement during challenging times.

Finally, I am deeply thankful to my family. Without their love, everything is impossible.